Quantum extension of the Kruskal spacetime

Abhay Ashtekar,[1] Javier Olmedo,[1] and Parampreet Singh[2]

[1]*Institute for Gravitation and the Cosmos, Penn State University, University Park, Pennsylvania 16801, USA*

[2]*Department of Physics and Astronomy, Louisiana State University, Baton Rouge, Louisiana 70803, USA*

A new description of macroscopic Kruskal black holes that incorporates the quantum geometry corrections of loop quantum gravity is presented. It encompasses both the "interior" region that contains classical singularities and the "exterior" asymptotic region. Singularities are naturally resolved by the quantum geometry effects of loop quantum gravity. The resulting quantum extension of spacetime has the following features: (i) It admits an infinite number of trapped, anti-trapped and asymptotic regions; (ii) All curvature scalars have uniform (i.e., mass independent) upper bounds; (iii) In the large mass limit, all asymptotic regions of the extension have the same ADM mass; (iv) In the low curvature region (e.g., near horizons) quantum effects are negligible, as one would physically expect; and (v) Final results are insensitive to the fiducial structures that have to be introduced to construct the classical phase space description (as they must be). Previous effective theories shared some but not all of these features. We compare and contrast our results with those of these effective theories and also with expectations based on the AdS/CFT conjecture. We conclude with a discussion of limitations of our framework, especially for the analysis of evaporating black holes.

I. INTRODUCTION

It is widely believed that predictions of general relativity cannot be trusted once spacetime curvature enters the Planck regime since modifications to Einstein's equations due to quantum gravity effects would then begin to dominate. In particular, singularities of classical general relativity are often regarded as windows onto new physics. In loop quantum gravity (LQG), new physics emerges from the underlying quantum Riemannian geometry (see, e.g., [1]) Thus, e.g., in the commonly used cosmological models singularities are naturally resolved because, once a curvature invariant approaches the Planck scale, quantum geometry modifications of Einstein dynamics introduce strong repulsive corrections that dilute that invariant, preventing a blowup [2,3].

It is then natural to ask if these quantum geometry effects also resolve black hole singularities. The simplest model is provided by the Schwarzschild-Kruskal spacetime. For the question of singularity resolution, it suffices to restrict oneself to the black hole region that is bounded by the singularity and event horizons, often referred to as the "Schwarzschild interior." Since this region is isometric to the (vacuum) Kantowski-Sachs cosmological model, one can transport LQG techniques developed for homogeneous but anisotropic cosmologies. Therefore, the Schwarzschild interior has drawn considerable attention from the LQG community (see, e.g., [4–17] for investigations closely

related to this paper). The general procedure used in all these investigations is the same: (a) The classical theory is cast in a Hamiltonian framework using connection variables; (b) the passage to quantum theory is through a representation of the fundamental commutation relations that descends from full LQG and, therefore, has inbuilt elements of quantum geometry; (c) the quantum Hamiltonian constraint is constructed by replacing curvature with holonomies of the gravitational connection around suitable loops that enclose minimum nonzero area allowed by quantum geometry; and, finally, (d) detailed physical predictions of the model are obtained using certain 'effective equations.'[1] Solutions to these equations show that the central singularity is resolved due to quantum corrections. We follow the same procedure. As we show in Sec. III, the singularity is replaced by a spacelike, three-dimensional transition surface $\mathcal{T}$ to the past of which we

---

[1]In the cosmological models, effective equations were first introduced by examining the form of the quantum Hamiltonian constraint, then writing down an effective Hamiltonian constraint on the *classical* phase space that includes key quantum corrections due to quantum geometry effects of LQG, and calculating its dynamical flow, again on the classical phase space. Later these equations were shown to follow from the full quantum dynamics of sharply peaked states [3,18,19]. In the Schwarzschild case, this last step has not been carried out in any of the approaches, including ours.

126003-1

have a trapped region (as in the Schwarzschild-Kruskal black hole region) and to the future of which is an antitrapped region (as in the Schwarzschild-Kruskal white hole region).

However, the analyses [4–17] differ in the way step (C) is implemented in detail. Consequently, the resulting effective dynamics of step (D) varies from one approach to another. Subsequent investigations have revealed that these effective descriptions have undesirable or puzzling features whose physical origin has remained unclear. For example, physical effects fail to be independent of the fiducial structure introduced to construct the classical phase space in some approaches [4,5,8], while quantum geometry effects could be large in low curvature regimes in other approaches. In particular, the quintessentially quantum transition surface could emerge in a low curvature region for macroscopic black holes with large masses [10,12]. Similarly, spacetime geometry near the black hole horizon could receive large quantum corrections even when the mass of the black hole is very large and hence the curvature near its horizon is low [6,7,13].[2] A systematic discussion of these limitations, including their origin, is given in Secs. IV D (and VI).

To compare and contrast these investigations, it is convenient to divide them into three broad classes, in terms of their method of selecting the loops needed in step (C). In all these treatments, the loops are characterized by two quantum parameters, labeled δ_b and δ_c. In [4,5,8], these parameters are set to a constant; in [10,12] they are certain Dirac observables, i.e., functions on phase space that are constant along (effective) dynamical trajectories; and in [6,7,9,11,13,20,21] they are more general functions on the classical phase space that change not only from one dynamical trajectory to another but also along each individual trajectory. The overall strategy we will adopt is the same as that in [10] but the specific Dirac observables we use are chosen more judiciously, using conditions that refer to the transition surface $\mathcal{T}$. As a result, unlike in [10], the transition surface $\mathcal{T}$ always lies in the Planck regime in our effective theory, and there is also excellent agreement with classical general relativity in low curvature regions. The trapped and antitrapped regions are joined smoothly to asymptotic regions, leading to a genuine quantum extension of the full Kruskal spacetime beyond classical singularities. (For a Penrose diagram of the full extension, see Fig. 4).

There is another key difference from previous investigations. The primary focus there was on Kantowski-Sachs spacetimes, with emphasis on issues that feature prominently in anisotropic *cosmologies*, such as bounces of various scale factors [6,9–11,13,20], behavior of the energy density, expansion scalar, shear potentials of the Weyl curvature [21], and, geodesic completeness and generic resolution of strong singularities [22]. Some of the discussions also included matter sources [20–22] or a cosmological constant [9,11]. While the inclusion of matter is natural from the cosmological perspective, the analysis no longer has direct relevance for quantum modifications of the Schwarzschild geometry near its singularity. Finally, a limitation of all existing studies of loop quantization of the Schwarzschild interior is that effective geometry is not extended to the asymptotic regions. By contrast, the object of primary interest to this investigation is the Kruskal spacetime, and the emphasis is on the corresponding spacetime notions, such as trapped and antitrapped regions, black hole–type and white hole–type horizons, the corresponding asymptotic regions, and the behavior of the static Killing field as one passes from the original Kruskal spacetime to its quantum extension. In particular, we also introduce an effective description in the asymptotic regions and show that the effective metric in the asymptotic and interior regions match at the horizons.

Material is organized as follows. Section II fixes the notation used subsequently, recalls the basics of the Hamiltonian framework, and summarizes the effective equations and their solutions. This discussion is included to make the paper self-contained. In Sec. III, we shift the focus from phase space trajectories to spacetime geometry and discuss the causal structure of the effective spacetime metric. As one might expect, corrections to the classical geometry are large in the regime where spacetime curvature enters Planck scale. As a result, a transition surface $\mathcal{T}$ with regular spacetime geometry now emerges, separating trapped and antitrapped regions. There is a precise sense in which $\mathcal{T}$ replaces the classical singularity in the quantum corrected, effective geometry. In Sec. IV, we motivate and introduce our specific choice of the quantum parameters δ_b, δ_c and discuss various features of the resulting effective spacetime geometry in the extended Schwarzschild interior. In Sec. V, we introduce the effective description in the exterior, asymptotic region of Schwarzschild spacetime and show that this effective metric matches smoothly to that in the interior.[3] For macroscopic black holes spacetime curvature is small near horizons. As one would hope on physical grounds, quantum corrections are also small near horizons in both interior and exterior regions and further decay rapidly as one moves away from the horizon in the asymptotic region. In Sec. VI, we summarize our main results and contrast our approach and findings with those used in previous investigations in LQG and also with the expectations based on the AdS/CFT correspondence [26].

---

[2]The same turns out to be true for the δ_b, δ_c prescriptions studied in Refs. [20,21] in the context of Kantowski-Sachs cosmologies, when they are used to model the Schwarzschild interior.

[3]Another approach that incorporates both the interior and the exterior regions of Schwarzschild but without making a direct use of homogeneity is summarized in [23]. This approach has also been used to study effects of quantum geometry on Hawking radiation [24], and collapse of self-gravitating shells [25].

We conclude with a discussion of limitations of our analysis.

Since the LQG literature on quantum corrections to the Schwarzschild metric is spread over 10–15 years, we have made an attempt to make the paper self contained by recalling key ideas at various junctures. Throughout, one should bear in mind that effective descriptions can be expected to provide a good approximation to the quantum evolution only if the mass M of the black hole is large, i.e., $GM =: m \gg \ell_{\mathrm{Pl}}$, where ℓ_{Pl} is the Planck length. This is the regime of interest to this paper.

II. PRELIMINARIES

As explained in Sec. I, in the first part of the paper we will focus on the Schwarzschild interior and use the fact that this portion of the Kruskal spacetime is naturally foliated by a family of homogeneous spacelike 3-manifolds. One can, therefore, use techniques from loop quantum cosmology (LQC) to construct a Hamiltonian framework based on connection and triad variables, A_a^i and E_i^a, and then pass to the quantum theory using the same methods that are used in full LQG (see, e.g., [3]). In cosmological models, quantum dynamics leads to a nonsingular evolution in which matter density and curvature remain finite. Furthermore, one can extract an effective description [3,18,19] from the resulting quantum theory following a systematic procedure based on a geometrical formulation of quantum mechanics [27]. Rigorous numerical simulations have shown that the effective description provides an excellent approximation to the underlying quantum dynamics for isotropic [28–30], as well as anisotropic spacetimes [31] so long as we consider quantum states that are sharply peaked on "large" universes at late times.

For the Schwarzschild interior, one can also introduce quantum kinematics (see e.g., [4,10]) and write down the Hamiltonian constraint operator. However, for our choice of quantum parameters δ_b, δ_c, its explicit action is rather complicated (see Appendix A). Therefore, in this paper we will focus only on the effective description, leaving the exploration of its relation to full quantum dynamics for a future work. In contrast to previous investigations of effective dynamics, our emphasis will be more on the causal structure and geometric properties of the quantum corrected spacetime than on phase space trajectories and cosmological issues associated with the Kantowski-Sachs spacetime. The purpose of this section is to summarize this procedure. We begin with the phase space and classical dynamics and then discuss effective dynamics. Our treatment and conventions are based on Refs. [4,10], which the reader can refer to for further details.

A. Phase space and classical dynamics

Recall that the interior of the Kruskal spacetime is isometric to the Kantowski-Sachs vacuum solution.

The homogeneous Cauchy slices have topology $\mathbb{R} \times \mathbb{S}^2$. As is customary in the phase space formulation of homogeneous models, let us introduce a fiducial metric $\mathring{q}_{ab}$ on Σ

$$\mathring{q}_{ab}\mathrm{d}x^a\mathrm{d}x^b = \mathrm{d}x^2 + r_o^2(\mathrm{d}\theta^2 + \sin^2 \mathrm{d}\phi^2), \quad (2.1)$$

where $x \in (-\infty, \infty)$, θ and ϕ are 2-sphere coordinates, and r_o is a constant (with dimensions of length). Since Σ is noncompact in the x direction, and all fields under consideration are homogeneous, in the construction of the phase space description we need to introduce an infrared cut-off; otherwise expressions of the symplectic structure and the (integrated) Hamiltonian constraint would be divergent. This is achieved by introducing a fiducial cell $\mathcal{C}$ in Σ, also with topology $\mathbb{R} \times \mathbb{S}^2$, but with $x \in (0, L_o)$. In the phase space considerations, all fields and integrals will be restricted to $\mathcal{C}$. Although intermediate structures will refer to L_o, the final physical results–such as equations of motion–will be independent of this choice in our classical as well as effective theory.

Using the underlying spatial homogeneity of the Kantowski-Sachs spacetime, we can solve the spatial diffeomorphism constraint and perform a partial gauge fixing to satisfy the Gauss constraint. As a result, the gravitational connection and the conjugate densitized triad can be expressed as

$$A_a^i\tau_i\mathrm{d}x^a = \bar{c}\tau_3\mathrm{d}x + \bar{b}r_o\tau_2\mathrm{d}\theta - \bar{b}r_o\tau_1 \sin\theta\mathrm{d}\phi + \tau_3 \cos\theta\mathrm{d}\phi,$$
$$(2.2)$$

and

$$E_i^a\tau^i\partial_a = \bar{p}_c r_o^2\tau_3 \sin\theta\partial_x + \bar{p}_b r_o\tau_2 \sin\theta\partial_\theta - \bar{p}_b r_o\tau_1\partial_\phi.$$
$$(2.3)$$

Here τ_i are SU(2) generators related to Pauli spin matrices σ_i via $\tau_i = -i\sigma_i/2$, and the constants $\bar{b}, \bar{c}, \bar{p}_b, \bar{p}_c$ represent the dynamical variables. Thus, the symmetry reduced phase space is now coordinatized by two configuration variables $(\bar{b}, \bar{c})$ and their conjugate momenta $(\bar{p}_b, \bar{p}_c)$. The symplectic structure is given by

$$\bar{\Omega} = \frac{L_o r_o^2}{2G\gamma}(2\mathrm{d}\bar{b} \wedge \mathrm{d}\bar{p}_b + \mathrm{d}\bar{c} \wedge \mathrm{d}\bar{p}_c), \quad (2.4)$$

where γ is the Barbero-Immirzi parameter that captures the quantization ambiguity in LQG.[4] The symplectic structure

---

[4]The parameter γ arises in the passage from classical to quantum theory. In quantum theory, it determines the LQG area gap Δ via $\Delta = 4\sqrt{3}\pi\gamma\ell_{\mathrm{Pl}}^2$. Its value is generally fixed to be $\gamma = 0.2375$ using black hole entropy considerations. Although in the final picture one can get rid of γ in favor of the more fundamental and physical parameter Δ, both parameters feature in various expressions in the existing literature [4–7,10]. To facilitate comparison we will also keep both parameters.

depends explicitly on the length L_o of the fiducial cell and the radius r_o in the fiducial metric $\overset{\circ}{q}_{ab}$. We can absorb L_o and r_o by rescaling the connection and triad variables: $b = r_o \bar{b}$, $c = L_o \bar{c}$, $p_b = L_o r_o \bar{p}_b$ and $p_c = r_o^2 \bar{p}_c$. They then satisfy the following Poisson brackets:

$$\{c, p_c\} = 2G\gamma, \qquad \{b, p_b\} = G\gamma. \qquad (2.5)$$

Note that under the transformation $r_o \to \beta r_o$ (where β is a constant) the rescaled connection and triad variables are invariant. However, under a rescaling of fiducial length L_o: $L_o \to \alpha L_o$ (where α is a constant), we get $b \to b$, $c \to \alpha c$, $p_b \to \alpha p_b$ and $p_c \to p_c$. Therefore, physical quantities can depend only on b, p_c and the combinations c/L_o and p_b/L_o.

The gravitational connection and spatial triads now take the form:

$$A_a^i \tau_i dx^a = \frac{c}{L_o}\tau_3 dx + b\tau_2 d\theta - b\tau_1 \sin\theta d\phi + \tau_3 \cos\theta d\phi, \qquad (2.6)$$

and

$$E_i^a \tau^i \partial_a = p_c \tau_3 \sin\theta \partial_x + \frac{p_b}{L_o}\tau_2 \sin\theta \partial_\theta - \frac{p_b}{L_o}\tau_1 \partial_\phi. \qquad (2.7)$$

Given any choice of a time coordinate τ and the associated lapse N_τ, each point in the phase space defines a spatially homogeneous metric with Kantowski-Sachs isometries via

$$g_{ab}dx^a dx^b \equiv ds^2 = -N_\tau^2 d\tau^2 + \frac{p_b^2}{|p_c|L_o^2}dx^2 + |p_c|(d\theta^2 + \sin^2\theta d\phi^2). \qquad (2.8)$$

Therefore, by restricting ourselves to $\tau < 2m$, we can use the standard form of the interior Schwarzschild solution

$$ds^2 = -\left(\frac{2m}{\tau} - 1\right)^{-1}d\tau^2 + \left(\frac{2m}{\tau} - 1\right)dx^2 + \tau^2(d\theta^2 + \sin^2\theta d\phi^2), \qquad (2.9)$$

(where $m = GM$) to set up a dictionary between phase space variables and their spacetime counterparts.[5] In terms of m and the radius τ of metric 2-spheres, we have $|p_c| = \tau^2$, $p_b^2 = L_o^2(\frac{2m}{\tau} - 1)\tau^2$ and $N_\tau^2 = (\frac{2m}{\tau} - 1)^{-1}$.

With the Gauss and spatial diffeomorphism constraint fixed, we can extract classical dynamics from the Hamiltonian constraint using Hamilton's equations.

It turns out that in the effective theory there is a particularly convenient choice of lapse for which dynamical equations simplify sufficiently to obtain explicit solutions [10]. The classical analog of that lapse is

$$N_{cl} = \gamma b^{-1}\text{sgn}(p_c)|p_c|^{1/2}, \qquad (2.10)$$

and we will denote the corresponding time variable by T_{cl}. The corresponding Hamiltonian constraint is

$$H_{cl}[N_{cl}] = -\frac{1}{2G\gamma}\left(2cp_c + \left(b + \frac{\gamma^2}{b}\right)p_b\right). \qquad (2.11)$$

Using Hamilton's equations, the evolution equations for connection variables turn out to be

$$\dot{b} = G\gamma \frac{\partial H_{cl}[N_{cl}]}{\partial b} = -\frac{1}{2b}(b^2 + \gamma^2), \quad \text{and}$$

$$\dot{c} = 2G\gamma \frac{\partial H_{cl}[N_{cl}]}{\partial c} = -2c, \qquad (2.12)$$

where the 'dot' denotes time derivative with respect to T_{cl}. Similarly, for the triad variables we obtain,

$$\dot{p}_b = -G\gamma \frac{\partial H_{cl}[N_{cl}]}{\partial p_b} = \frac{p_b}{2b^2}(b^2 - \gamma^2), \quad \text{and}$$

$$\dot{p}_c = 2G\gamma \frac{\partial H_{cl}[N_{cl}]}{\partial p_c} = 2p_c. \qquad (2.13)$$

Solutions to these dynamical equations together with the Hamiltonian constraint turn out to be

$$b(T_{cl}) = \pm\gamma(e^{-T_{cl}} - 1)^{1/2}, \qquad c(T_{cl}) = \mp c_o e^{-2T_{cl}}, \qquad (2.14)$$

and

$$p_b(T_{cl}) = p_b^{(o)}e^{T_{cl}}(e^{-T_{cl}} - 1)^{1/2}, \qquad p_c(T_{cl}) = p_c^{(o)}e^{2T_{cl}}. \qquad (2.15)$$

In writing these solutions, we have fixed one of the integration constants so that, in the spacetime picture, the black hole horizon lies at $T_{cl} = 0$. The singularity now occurs at $T_{cl} = -\infty$ so that the Schwarzschild interior corresponds to $-\infty < T_{cl} < 0$. The remaining three integration constants, c_o, $p_b^{(o)}$ and $p_c^{(o)}$ are subject to one condition coming from the Hamiltonian constraint $H_{cl}[N_{cl}] = 0$ and can, therefore, be parametrized by two constants, m, L_o [4,10]: $c_o = \gamma L_o/4m$; $p_b^{(o)} = -2mL_0$; $p_c^{(o)} = 4m^2$. Here, and in what follows we fix the orientation of the spatial triad [see (2.7)] and restrict ourselves to $p_c \geq 0, c > 0, b > 0$ and $p_b \leq 0$.

---

[5]We have used the notation that is tailored to the Schwarzschild interior. The standard Schwarzschild form is obtained by substitutions $\tau \to r$ and $x \to t$.

The form of the solutions immediately implies that $cp_c/(L_o\gamma)$ is a Dirac observable–i.e., a constant of motion–that equals $m = GM$ in the spacetime metric defined by the dynamical trajectory:

$$\frac{cp_c}{L_o\gamma} = m \quad \text{along any classical dynamical trajectory.} \tag{2.16}$$

Finally, to display the standard form (2.9) of the metric, it suffices to change the time coordinate and set $\tau := 2me^{T_{cl}}$. At the horizon, identified by $\tau = 2m$, or $T_{cl} = 0$, we have $b = 0$ and $p_b = 0$ and c and p_c take the values, $c(0) = \gamma L_o/4m$ and $p_c(0) = 4m^2$. The central singularity occurs at $\tau = 0$ or $T_{cl} \to -\infty$. Here the connection components diverge and both of the triad components vanish.

B. Effective dynamics

Effective equations are formulated on the same phase space as the one used in the classical theory but they incorporate leading order quantum corrections through 'quantum parameters' δ_b, δ_c. As mentioned in Sec. I, we will assume that: (1) δ_b and δ_c are judiciously chosen Dirac observables (and, thus, commute with the Hamiltonian constraint); and, (2) go to zero in the limit in which the area gap Δ is sent to zero. Condition (1) is a subtle requirement because $H_{eff}(N)$ itself depends on δ_b, δ_c [see Eq. (2.18)]. However, as our discussion in Appendix A (and Sec. IV A) shows, a large family of consistent choices does exist. Thus, δ_b, δ_c will be $\hbar$-dependent phase space functions which remain constant along dynamical trajectories. A specific choice will be made in Sec. III, and it will ensure $\delta_b \ll 1$ and $\delta_c \ll 1$ for macroscopic black holes.

Now, as mentioned in Sec. II A, a convenient choice of lapse considerably simplifies the analysis of effective dynamics and enables one to write solutions in a closed analytic form. Therefore, following [10], we will set[6]

$$N = \frac{\gamma \operatorname{sgn}(p_c)|p_c|^{1/2}\delta_b}{\sin(\delta_b b)}, \tag{2.17}$$

and we will denote the corresponding time variable by T. (Just as $T_{cl} < 0$ in the Schwarzschild 'interior', we will see that $T < 0$ in the 'extended Schwarzschild interior' because as in the classical theory N blows up at $T = 0$.) The resulting effective Hamiltonian is given by

---

[6]In the quantum theory, only holonomies defined by the connection are well defined; not the connections themselves. As in LQC, holonomies are almost periodic functions of connections and we are led to restrict the phase space to the sector $\delta_b b \in (0, \pi); \delta_c c \in (0, \pi); p_b < 0$ and $p_c > 0$, where the last two conditions are the same as in the classical theory.

$$H_{eff}[N] = -\frac{1}{2G\gamma}\left[2\frac{\sin(\delta_c c)}{\delta_c}|p_c| + \left(\frac{\sin(\delta_b b)}{\delta_b} + \frac{\gamma^2\delta_b}{\sin(\delta_b b)}\right)p_b\right]. \tag{2.18}$$

It is easy to see that in the classical limit $\delta_b \to 0$ and $\delta_c \to 0$, the lapse N in the effective theory agrees with the lapse N_{cl} in the classical theory [see Eqs. (2.17) and (2.10)], and the effective Hamiltonian $H_{eff}[N]$ reduces to the classical Hamiltonian (2.11). As shown in Appendix A, there exists a class of quantum parameters δ_b, δ_c which lead to the following dynamical equations for connection and triad components:

$$\dot{b} = -\frac{1}{2}\left(\frac{\sin(\delta_b b)}{\delta_b} + \frac{\gamma^2\delta_b}{\sin(\delta_b b)}\right), \qquad \dot{c} = -2\frac{\sin(\delta_c c)}{\delta_c}, \tag{2.19}$$

and

$$\dot{p}_b = \frac{p_b}{2}\cos(\delta_b b)\left(1 - \frac{\gamma^2\delta_b^2}{\sin^2(\delta_b b)}\right), \quad \dot{p}_c = 2p_c\cos(\delta_c c), \tag{2.20}$$

where the 'dot' denotes derivative with respect to T.

An interesting feature of the above set of equations is that dynamics of b and p_b decouples from that of c and p_c. Thus, the trajectories for the (b, p_b) sector in the effective phase space can be obtained independently from the trajectories for the (c, p_c) sector. This feature, which is shared with the classical theory, is tied to δ_b and δ_c being Dirac observables and plays a crucial role in obtaining closed form solutions in the effective theory. If δ_b and δ_c had been general phase space functions dynamical equations would become intricately coupled and have to be solved numerically as in [6,7,11,21].

It is straightforward to integrate these Hamilton's equations for b, c and p_c variables. The strategy is to solve the (c, p_c) sector first, then the dynamical equation for b and finally obtain the solution for p_b using the vanishing of the effective Hamiltonian constraint $H_{eff} \approx 0$. The general solution is:

$$\tan\left(\frac{\delta_c c(T)}{2}\right) = \mp\frac{\gamma L_o\delta_c}{8m}e^{-2T}, \tag{2.21}$$

$$p_c(T) = 4m^2\left(e^{2T} + \frac{\gamma^2 L_o^2\delta_c^2}{64m^2}e^{-2T}\right), \tag{2.22}$$

$$\cos(\delta_b b(T)) = b_o\tanh\left(\frac{1}{2}\left(b_o T + 2\tanh^{-1}\left(\frac{1}{b_o}\right)\right)\right), \tag{2.23}$$

where

$$b_o = (1 + \gamma^2 \delta_b^2)^{1/2}, \qquad (2.24)$$

and,

$$p_b(T) = -2 \frac{\sin(\delta_c c(T))}{\delta_c} \frac{\sin(\delta_b b(T))}{\delta_b} \frac{p_c(T)}{\frac{\sin^2(\delta_b b(T))}{\delta_b^2} + \gamma^2}. \qquad (2.25)$$

Note that in the classical limit $\delta_b \to 0$ and $\delta_c \to 0$, these solutions reduce to (2.14) and (2.15). Next, (2.21) and (2.22) immediately imply that $p_c \sin(\delta_c c)/(\gamma L_o \delta_c)$ is a Dirac observable which, in the classical limit, has interpretation of the mass m of the black hole. Since, as we will see, our effective theory agrees with the classical theory in the low curvature region (e.g., near the black hole horizon for macroscopic black holes) and since Dirac observables are constants of motion, we will denote it again by m. Thus, in our effective theory:

$$m := \left[\frac{\sin \delta_c c}{\gamma L_o \delta_c} \right] p_c, \qquad (2.26)$$

which can also be expressed using only b, p_b on the constraint surface [see Eq. (2.18)]:

$$m := -\frac{1}{2\gamma} \left[\frac{\sin \delta_b b}{\delta_b} + \frac{\gamma^2 \delta_b}{\sin \delta_b b} \right] \frac{p_b}{L_o}. \qquad (2.27)$$

One can pass from the phase space to the spacetime description following the same procedure as in the classical theory. Thus, the quantum corrected spacetime metric is given by substituting the lapse N of (2.17) and solutions (2.22) and (2.25) for triads p_c, p_b in the expression (2.8).

An important feature of the effective dynamics is that the solutions are nonsingular so long as the appropriately chosen quantum parameters δ_b and δ_c are nonzero. In the classical theory, the connection components diverge and the triad components go to zero at the singularity. This does not occur anywhere in the effective spacetime metric. In particular, p_c takes a minimum value $p_c|_{\min} = m\gamma L_o \delta_c$ in every effective spacetime. In the phase space picture, the triad p_c bounces avoiding the central singularity. This singularity resolution is a direct manifestation of the nonperturbative quantum gravitational effects encoded in the effective Hamiltonian via quantum parameters δ_b and δ_c.

To summarize, there is a large class of judiciously chosen quantum parameters δ_b, δ_c (discussed in Appendix A) that lead to the quantum corrected, effective spacetime geometry given by Eqs. (2.8), (2.2), (2.25). To make a more detailed investigation of properties of the quantum

corrected, effective spacetime one has to specify δ_b and δ_c. We will do this in Sec. IV.

III. CAUSAL STRUCTURE OF THE EFFECTIVE SPACETIME GEOMETRY

As we remarked in Sec. I, previous discussions of singularity resolution treated Schwarzschild interior as a cosmological model and focused on issues that are at forefront in anisotropic models, such as bounces of scale factors. Our focus, by contrast, is on black hole aspects. Therefore, we will now investigate the consequences of the phase space dynamics of Sec. II B on the spacetime geometry. Specifically, we will analyze the causal structure in the extension of Schwarzschild interior provided by the effective metric and show that it is divided by a trapped and antitrapped regions, separated by a three-dimensional spacelike transition surface $\mathcal{T}$ that replaces the classical singularity. Results of this section are general in the sense that they are not tied to the specific choice of the quantum parameters introduced in Sec. IV; they are consequences of equations of motion (2.21)–(2.25) that hold for any δ_b, δ_c in the large family discussed in Appendix A.

Let us begin by recalling the situation in the classical theory. There, the spacetime metric (2.9) corresponding to every dynamical trajectory (with nonzero m) admits a black hole (BH) horizon at time $\tau = 2m$, or $T = 0$, where the translational Killing vector field X^a (with $X^a \partial_a = \partial/\partial_x$) becomes null and the spatial 3-metric becomes degenerate. In the phase space description, the horizon is characterized by conditions $b = 0$, $p_b = 0$ [see Eqs. (2.14) and (2.15)]. At these points, the lapse $N_{\rm cl}$ of Eq. (2.10) diverges and so the interpretation in terms of spacetime geometry breaks down. Therefore, the horizon represents the past boundary of the interior region. Each dynamical trajectory also has a future end point at which p_c vanishes ($\tau = 0$ or $T = -\infty$) [see Eq. (2.15)]. In terms of spacetime geometry, these points represent the future singularity at which b, c and the Kretschmann scalar diverge.

Let us now examine how this situation changes in the quantum corrected, effective spacetime geometry. By construction, the effective metric (2.8) is again spherically symmetric and has a spacelike translational Killing vector field X^a. Thus, as in the classical theory, the spacetime under consideration is foliated by homogeneous, spacelike Cauchy surfaces. The past boundary is again represented by the phase space points $b = 0$, $p_b = 0$ at which the lapse N of Eq. (2.17) diverges. (Note that, as in the classical theory, along dynamical trajectories vanishing of b implies vanishing of p_b and divergence of N. See Eqs. (2.25) and (2.17).) The form (2.8) of the metric implies that the Killing vector field X^a becomes null there.

However, as we already noted in Sec. II B, Eq. (2.22) implies that p_c now admits a nonzero minimum value, $p_c^{\min} = \frac{1}{2}\gamma(L_o \delta_c)m$ along every dynamical trajectory. (Recall that p_c and $L_o \delta_c$ are both invariant under the

rescalings of the fiducial cell and the fiducial metric.) As a consequence, none of the curvature scalars diverges: the spacetime metric defined by the effective dynamical trajectory is smooth. In the spacetime picture, the 3-surface $\mathcal{T}$ on which p_c achieves its minimum replaces the classical singularity in the quantum corrected geometry. To discuss geometrical properties of $\mathcal{T}$, let us begin by introducing the two future pointing null normals $\ell_\pm^a$ to the metric 2-spheres $x = $ const and $T = $ const:

$$\ell_a^\pm = \alpha_\pm \nabla_a T \pm \beta_\pm \nabla_a x. \qquad (3.1)$$

The standard normalization conditions

$$g^{ab}\ell_a^\pm \ell_a^\pm = 0, \qquad g^{ab}\ell_a^+\ell_a^- = -1, \qquad (3.2)$$

with $\alpha_\pm > 0$ and $\beta_\pm > 0$, fix three of the parameters $\alpha_\pm$ and $\beta_\pm$ and we will fix the remaining freedom by setting $\alpha_+ = 1$. The expansions of these null vectors can be expressed in terms of phase space variables as

$$\theta_\pm = S^{ab}\nabla_a \ell_b^\pm = N^2 \dot{p}_c, \qquad (3.3)$$

where S^{ab} is the projection operator on the metric 2-spheres. Since N cannot vanish [see Eq. (2.17)], either of the two expansions $\theta_\pm$ vanishes if and only if $\dot{p}_c = 0$, and then they both vanish. It follows from (2.22) that each effective trajectory in the phase space admits one and only one point at which this occurs, and the corresponding time coordinate in the spacetime description is given by

$$T_{\mathcal{T}} = \frac{1}{2}\ln\left(\frac{\gamma L_o \delta_c}{8m}\right). \qquad (3.4)$$

To the past of the 3-surface $T = T_{\mathcal{T}}$—i.e., in the region $0 > T > T_{\mathcal{T}}$—both expansions $\theta_\pm$ are negative; i.e., the metric 2-spheres are all trapped. To the future of this surface–i.e., for $T_{\mathcal{T}} > T$, both expansions $\theta_\pm$ are positive; i.e., the metric 2-spheres are all antitrapped. (Recall that, by its definition, the coordinate T decreases from $T = 0$ as we go to the future in the spacetime picture and is, thus, negative in the entire spacetime region of interest.) Therefore, $\mathcal{T}$ is the transition surface from trapped region to antitrapped region of the spacetime metric (2.8).[7] Since $\dot{p}_c$ has precisely one zero along each dynamical trajectory, each solution admits one and only one transition surface. What happens to $\mathcal{T}$ in the classical limit $\delta_b \to 0$ and

$\delta_c \to 0$? In that case $T_{\mathcal{T}} \to -\infty$ which corresponds to the classical black hole singularity. In his precise sense, in the effective description $\mathcal{T}$ replaces the classical singularity.

What is the nature of the spacetime geometry to the future of the transition surface $\mathcal{T}$? Since both expansions $\theta_\pm$ are now positive, the causal structure is completely analogous to the white hole region of Kruskal spacetime. In this sense, one can say that $\mathcal{T}$ marks a transition from a black hole interior to the white hole interior. However, we will refrain from using this terminology because to some it suggests that the black hole singularity still persists and the extension corresponds to attaching a white hole geometry to the future of the singularity. We emphasize that the entire geometry is smooth and $\mathcal{T}$ is invariantly defined as the boundary between a trapped region in the past to an antitrapped region to the future.

As we saw, the past boundary of the spacetime region defined by effective trajectories in our phase space has the interpretation of the black hole horizon since the Killing field X^a becomes null there. Since the future of $\mathcal{T}$ represents an antitrapped region, it is natural to ask if this region also admits a boundary that can be interpreted as the white hole horizon. It follows from the form of the metric (2.8) that, as in the classical theory, if $p_b(T_0)$ vanishes, then the surface $T = T_0$ would represent a Killing horizon. Equation (2.25) implies that this occurs at $T_0 = -(4/b_o) \times \tanh^{-1}(1/b_o)$ because then $\delta_b b(T_0) = \pi$ whence $p_b = 0$. We will see in Sec. IV that for macroscopic black holes this occurs in a low curvature region with our choice of the quantum parameters δ_b, δ_c. Thus, in our effective theory, the extended Schwarzschild interior is the smooth spacetime region $T_0 < T < 0$ with a black hole–type horizon at $T = 0$ as its past boundary and a white hole–type horizon at $T = T_0$ as its future boundary. This portion of the effective spacetime is divided into a trapped region to the past of $\mathcal{T}$ and an antitrapped region to the future of $\mathcal{T}$.

Remarks: 1. Recall that the transition surface $\mathcal{T}$ in spacetime corresponds to the phase space point at which p_c bounces in the corresponding dynamical trajectory. The other phase space momentum variable p_b appears only in the expression of the norm of the translational Killing field X^a in spacetime. It also undergo bounces and this generically occurs away from $\mathcal{T}$. We did not discuss these bounces since these are not significant for the causal structure of the effective spacetime under consideration.

2. The past boundary of the extended Schwarzschild interior is a black hole–type (i.e., future) horizon of the classical spacetime we started with, while the future boundary is a white hole–type (i.e., past) horizon. We will refer to them as black hole–or white hole–type rather than future or past horizons because, in the extended spacetime, the black hole–type future horizon lies to the past of the white hole–type past horizon (see Fig. 4).

---

[7]$\mathcal{T}$ has very interesting geometry. It is a spacelike 3-manifold that is foliated by marginally trapped surfaces. However, it is not a dynamical horizon because both expansions $\theta_\pm$ vanish on $T_{\mathcal{T}}$. Similarly, although the area of all marginally trapped 2-spheres is the same, $\mathcal{T}$ is *not* a nonexpanding horizon because it is spacelike. These features are quite exceptional: Indeed, we are not aware of any physically interesting spacetime in classical general relativity which admits a surface with these interesting properties.

IV. QUANTUM CORRECTED SPACETIME GEOMETRY OF THE SCHWARZSCHILD INTERIOR

This section is organized as follows. In Sec. IV A, we motivate and specify our choice of quantum parameters δ_b, δ_c. In Sec. IV B, we probe the nature of quantum corrections to Einstein's equations that are responsible for the singularity resolution. Even though there is no physical matter anywhere, it is often convenient to reinterpret nonvanishing of the Einstein tensor in terms of an effective stress energy tensor $\mathfrak{T}_{ab}$ induced by quantum geometry. We present expressions of the resulting effective energy density ρ and radial and tangential pressures $\mathfrak{p}_x$, $\mathfrak{p}_\parallel$, and show that the strong energy condition is indeed violated by this $\mathfrak{T}_{ab}$ in a neighborhood of the transition surface $\mathcal{T}$. In this neighborhood, then, there are large departures from classical general relativity. In Sec. IV C, we show that the spacetime curvature near $\mathcal{T}$ is of Planck scale. Interestingly, as is common in LQC, each curvature invariant has an absolute upper bound, i.e., one that does not depend on how large the mass is. This is in sharp contrast with the situation in classical general relativity, where the Kretschmann scalar $K(T) = 48m^2/p_c^3(T)$ grows with mass at any given T, making the 'strength' of the central singularity proportional to m^2. Finally, the effective stress-energy tensor $\mathfrak{T}_{ab}$ decays away from the transition surface $\mathcal{T}$ and becomes quickly negligible. Thus, for large m, Einstein's vacuum equations are satisfied to a high level of accuracy near the black hole–and white hole–type horizons. The overall situation is similar to that in LQC: quantum geometry corrections are negligible in low curvature regime but grow quickly in the Planck regime, creating an effective repulsive force that resolves the singularity. Finally, in Sec. IV D, we compare and contrast our strategy of fixing δ_b, δ_c and the results that follow with previous work on the singularity resolution in loop quantization of Kantowski-Sachs model [4–13,20,21].

A. Transition surface, area gap and δ_b, δ_c

As indicated in Sec. I, several different choices of quantum parameters δ_b, δ_c have been made in the literature [4–13], including those where δ_b and δ_c are not constants [6,7,9,11,13], leading to quite different effective descriptions of Schwarzschild interior. In this subsection, we will first motivate and then specify our choice. In Sec. IV D, we will compare and contrast the physical predictions that result from different choices.

Recall from Sec. II that the gravitational connection $A_a^i\tau_i$ enters in the Hamiltonian constraint via its curvature $F_{ab}^i\tau_i$. In the passage to quantum theory, there is a surprising result: the requirement of background independence selects a unique representation of the canonical commutation relations (in full LQG [32,33], as well as in LQC [34,35]). In this representation, there is no operator

corresponding to the connection $A_a^i\tau_i$ itself; only the operators corresponding to the holonomies h_ℓ defined by $A_a^i\tau_i$ along links ℓ are well defined. Therefore, in the quantum theory components of the curvature $F_{ab}^i\tau_i$ have to be expressed using holonomies (see, e.g., [1,36]). In the classical theory, one can calculate, say, $F_{\theta,\phi}^i\tau_i$ as follows: first evaluate the ratio $(h_{\square(\theta,\phi)} - 1)/(\text{Ar}(\square(\theta,\phi)))$—where $h_{\square(\theta,\phi)}$ is the holonomy around a closed rectangular plaquette $\square(\theta,\phi)$ within the θ-ϕ 2-sphere enclosing an area $\text{Ar}(\square(\theta,\phi))$—and then take the limit as the plaquette $\square(\theta,\phi)$ shrinks to a point. The idea is to use this procedure also in the quantum theory. However, the area operator has a discrete spectrum in LQG and there is a minimum nonzero area eigenvalue–the area gap Δ. Therefore, the strategy is to obtain the quantum operator corresponding to the classical curvature component $F_{\theta,\phi}^i\tau_i$ by shrinking the plaquette $\square(\theta,\phi)$ only till its area $\text{Ar}(\square(\theta,\phi))$ equals Δ. In the same manner, operators corresponding to the other two curvature components $F_{\phi,x}^i\tau_i$ and $F_{\theta,x}^i\tau_i$ are defined as holonomies along plaquettes $\square(\phi,x)$ and $\square(\theta,x)$ in the ϕ-x and θ-x planes enclosing area Δ. Therefore, we have:

$$\hat{F}_{ab}^i\tau_i = \frac{1}{\Delta}(h_{\square_{ab}} - 1), \qquad (4.1)$$

where the appropriately chosen plaquette $\square_{ab}$ lies in the a-b plane, enclosing area Δ. Consequently the operator corresponding to curvature now acquires a Planck scale nonlocality which lies at the heart of quantum corrections to dynamics that naturally resolve singularities.

The quantum parameter δ_b has the interpretation of the length of each link constituting the plaquette within the θ-ϕ 2-spheres, and δ_c, of the length of the links in the x direction within the plaquettes in the θ-x and ϕ-x planes in the fiducial cell $\mathcal{C}$. First investigations [4,5] of the Schwarzschild interior followed the procedure initially used in FLRW models [37]–known as the μ_o-scheme– and set δ_b, δ_c to a constant, δ [see footnote 1]. Later investigations revealed that the resulting quantum dynamics has several limitations [10,21]. (For example, its physical predictions depend on the choice of fiducial structures.) These were overcome in an 'improved dynamics' scheme in Ref. [6] (and a variant in Ref. [7]) by mimicking the successful '$\bar{\mu}$-scheme' introduced for the FLRW models in Ref. [28] (see Ref. [38] for a discussion about these two schemes). Then, δ_b, δ_c turn out to be specific functions on the phase space whose values evolve along the effective dynamical trajectories. However, as we discuss in Sec. IV D, effective theories based on all of these choices of δ_b, δ_c have physically unacceptable features. We, therefore, follow a procedure that straddles between the μ_o and $\bar{\mu}$ schemes: As mentioned before, our δ_b, δ_c will not be constants all over the phase space, but they will be constants along dynamical trajectories (as in [10]). That is,

they will Poisson-commute with the effective Hamiltonian constraint.

Our strategy is to fix the Dirac observables δ_b, δ_c by demanding that the plaquette $\Box(\theta, \phi)$ and $\Box(\phi, x)$ should enclose a minimum area when evaluated on $\mathcal{T}$. (By spherical symmetry, the condition is then satisfied also for the plaquette $\Box(\theta, x)$.) Our δ_b, δ_c will then be well defined Dirac observables because each effective trajectory admits one and only one point at which $\dot{p}_c = 0$ [which, in the effective spacetime geometry defines the transition surface $\mathcal{T}$; see Eq. (3.3)]. Now, since the parameters δ_b, δ_c used in the μ_o-type scheme [4,5] are constants on the entire phase space, they are also (trivially) Dirac observables. Our procedures differs from the μ_o scheme because we evaluate the area using the physical effective metric—rather than the fixed fiducial metric used in [4,5]—making crucial use of the transition surface $\mathcal{T}$. Therefore, our δ_b, δ_c are not constants on the phase space but vary from one effective dynamical trajectory to another.

Let us begin with an infinitesimal rectangular plaquette $\Box(\phi, x)$ in the $\theta = \pi/2$ plane of our fiducial cell. The plaquette has two parallel links along the x axis and two parallel links along $\theta = \pi/2$. Let δ_c denote the fractional length of the link along the x axis. Note that fractional lengths are metric independent. For example, with respect to the fiducial metric $\overset{\circ}{q}_{ab}$ of Eq. (2.1), the total length of the fiducial cell $\mathcal{C}$ along the x direction is L_o, and the length of our link will be $\delta_c L_o$. Similarly, with respect to the physical metric, the total length of the fiducial cell along the x direction is $(|p_b|/\sqrt{p_c})$ and the length of our link will be $(|p_b|/\sqrt{p_c})\delta_c$. Likewise, let the fractional length of the link along the equator be δ_b. Then, from the form (2.8) of the physical metric, we conclude that the *physical* area enclosed by the plaquette $\Box(\phi, x)$ at the transition surface $\mathcal{T}$ is:

$$\mathrm{Ar}(\Box(\phi, x)) = \delta_b \delta_c (2\pi |p_b||_{\mathcal{T}}). \qquad (4.2)$$

Since the total area $A_{\phi, x}$ of the ϕ-x plane in the fiducial cell is $2\pi |p_b|_{\mathcal{T}}$, as expected $\delta_b \delta_c$ has the invariant interpretation as the ratio of the area $\mathrm{Ar}(\Box(\phi, x))$ enclosed by the plaquette $\Box(\phi, x)$ and the total area of the ϕ, x-plane within the fiducial cell. We discussed these geometric properties in some detail to distinguish the present scheme from others in the literature. There, δ_b, δ_c are generally taken as coordinate lengths using θ, ϕ, x and so their invariant geometrical meaning remains unclear.[8]

---

[8]Also, this careful analysis is essential to get the correct 2π- and 4π-type numerical factors in the expressions of δ_b, δ_c in Eq. (4.6). Some of the physical properties depend on these factors. For example, in a less careful treatment that ignores these factors, the mass m changes as one moves from one asymptotic region to another one to its future (e.g., from region I to III in Fig. 4), even in the large mass limit.

Next, let us consider the plaquette $\Box(\theta, \phi)$ in any $x =$ const 2-sphere on the transition surface $\mathcal{T}$. Because the 2-spheres are round, we are led to use the same fractional length δ_b along the two orthogonal directions of the plaquette. Then it follows from the form (2.8) of the metric that the physical area enclosed by this plaquette on the transition surface $\mathcal{T}$ is

$$\mathrm{Ar}(\Box(\phi, x)) = (\delta_b)^2 (4\pi p_c|_{\mathcal{T}}), \qquad (4.3)$$

so that now $(\delta_b)^2$ has the interpretation of the ratio of the area enclosed by the plaquette to the total area of the 2-sphere.

We can now implement the main strategy: We will constrain δ_b, δ_c by requiring that the areas enclosed by the two plaquettes on the transition surface $\mathcal{T}$ be equal to the area gap:

$$2\pi \delta_c \delta_b |p_b||_{\mathcal{T}} = \Delta, \qquad (4.4)$$

and

$$4\pi \delta_b^2 p_c|_{\mathcal{T}} = \Delta. \qquad (4.5)$$

Since on each dynamical trajectory p_b and p_c have fixed values on the transition surface, it is intuitively clear that the two equations would determine the values of δ_b, δ_c. This is indeed the case under the well-motivated assumptions $\delta_b \ll 1$, $\delta_c \ll 1$ and $m \gg \ell_{\mathrm{Pl}}$ [where m is the phase space function defined in Eq. (2.26)]. Since the proof of this result is rather technical and requires a significant detour, to maintain the flow of the argument, we present it in Appendix B. The final result is that in the large m limit, we have

$$\delta_b = \left(\frac{\sqrt{\Delta}}{\sqrt{2\pi}\gamma^2 m}\right)^{1/3}, \qquad L_o \delta_c = \frac{1}{2}\left(\frac{\gamma \Delta^2}{4\pi^2 m}\right)^{1/3}. \qquad (4.6)$$

(Recall that it is only $L_o \delta_c$ that has invariant meaning in the sense of being independent of the choice of the fiducial metric and cell). Note that both parameters depend on mass and go as $m^{-\frac{1}{3}}$. This property is important for physical properties of the resulting effective metric.

B. Quantum corrections to Einstein's equations

From the perspective of classical general relativity it is natural to investigate how the effective theory manages to resolve the Schwarzschild singularity. The effective stress energy tensor induced by quantum corrections,

$$\mathfrak{T}_{ab} := \frac{1}{8\pi G} G_{ab}, \qquad (4.7)$$

must violate standard energy conditions. It is natural to ask: How large are the violations? and, Where do they occur? We will now discuss these issues.

Let us begin by noting that $\mathfrak{T}_{ab}$ can be interpreted as the stress energy tensor of an anisotropic perfect fluid with effective energy density

$$\rho = -\mathfrak{T}^0_0 = \frac{1}{8\pi G}\left(\frac{1}{p_c} + \frac{1}{N^2}\frac{\dot{p}_b\dot{p}_c}{p_b p_c} - \frac{1}{N^2}\frac{\dot{p}_c^2}{4p_c^2}\right), \quad (4.8)$$

and radial and tangential pressures

$$\mathfrak{p}_x = \mathfrak{T}^1_1 = \frac{1}{8\pi G}\left(-\frac{1}{p_c} + \frac{1}{N^2}\frac{\dot{p}_c^2}{4p_c^2} - \frac{1}{N^2}\frac{\ddot{p}_c}{p_c} + \frac{\dot{N}}{N^3}\frac{\dot{p}_c}{p_c}\right),$$
$$(4.9)$$

$$\mathfrak{p}_\| = \mathfrak{T}^2_2 = \frac{1}{8\pi G}\left(\frac{1}{N^2}\frac{\dot{p}_b\dot{p}_c}{2p_b p_c} - \frac{1}{N^2}\frac{\dot{p}_c^2}{4p_c^2} - \frac{1}{N^2}\frac{\ddot{p}_b}{p_b} + \frac{\dot{N}}{N^3}\frac{\dot{p}_b}{p_b}\right).$$
$$(4.10)$$

Since $\dot{p}_c = 0$ at the transition surface $\mathcal{T}$, we have

$$\left(\mathfrak{T}_{ab} - \frac{1}{2}g_{ab}\mathfrak{T}\right)T^a T^b\bigg|_{\mathcal{T}}$$
$$= (\rho + \mathfrak{p}_x + 2\mathfrak{p}_\|)|_{\mathcal{T}}$$
$$= \frac{1}{8\pi G}\left(\frac{\dot{N}}{N^3}\frac{2\dot{p}_b}{p_b} - \frac{1}{N^2}\frac{2\ddot{p}_b}{p_b} - \frac{1}{N^2}\frac{\ddot{p}_c}{p_c}\right)\bigg|_{\mathcal{T}}, \quad (4.11)$$

Note that the right-hand sides of (4.8)–(4.10) hold for any choice of lapse. Therefore, one can evaluate them using our choice (2.17) [using δ_b, δ_c as in (4.6)]. We find $\ddot{p}_c > 0$, $(\ddot{p}_b/p_b) > 0$, and $\dot{p}_b$ is much smaller than other terms in the expression, making the right side of (4.11) negative. (Indeed, as the plots in Figs. 2 show, ρ, $\mathfrak{p}_x$ and $\mathfrak{p}_\|$ are all negative at the transition surface for our choice of δ_b, δ_c, whence the middle term is manifestly negative.) Therefore, we conclude that

$$\left(\mathfrak{T}_{ab} - \frac{1}{2}g_{ab}\mathfrak{T}\right)T^a T^b\bigg|_{\mathcal{T}} < 0. \quad (4.12)$$

Thus, for macroscopic black holes considered in this paper, the strong energy condition is violated at (and, therefore, in a neighborhood of) $\mathcal{T}$, just as one would expect.

C. Universal upper bounds on curvature invariants

The explicit solutions to Hamilton's equations given in Sec. II B show that the phase space variables are manifestly finite along effective dynamical trajectories. Therefore, it is clear that the spacetime metric (2.8) is smooth throughout the open interior region bounded by the two horizons. Therefore, in any one effective solution, curvature scalars are all finite and, therefore, bounded above. However, these upper bounds could well diverge in the limit $m \to \infty$. Interestingly, this does not happen: each curvature invariant has an absolute, finite upper bound in this limit. Existence

of such *uniform* upper bounds appears to be a general occurrence in LQG. It could be a reflection of a deeper property of quantum geometry effects at the heart of the mechanism that leads to the resolution of strong, spacelike singularities in LQG [2,22].

Since we know the explicit time dependence of the phase space variables from Eqs. (2.21)–(2.25), using the form (2.8) of the spacetime metric we can calculate various curvature scalars at the transition surface. We used MATHEMATICA to simplify these expressions in the large m limit. The results can be summarized as follows: At the transition surface $\mathcal{T}$,

(i) the (square of the) Ricci scalar has the asymptotic form:

$$R^2|_{\mathcal{T}} = \frac{256\pi^2}{\gamma^4\Delta^2} + \mathcal{O}\left(\left(\frac{\ell_{\rm Pl}}{m}\right)^{\frac{2}{3}}\ln\frac{m}{\ell_{\rm Pl}}\right); \quad (4.13)$$

(ii) the square of the Ricci tensor has the asymptotic form

$$R_{ab}R^{ab}|_{\mathcal{T}} = \frac{256\pi^2}{\gamma^4\Delta^2} + \mathcal{O}\left(\left(\frac{\ell_{\rm Pl}}{m}\right)^{\frac{2}{3}}\ln\frac{m}{\ell_{\rm Pl}}\right); \quad (4.14)$$

(iii) the square of the Weyl tensor has the asymptotic form

$$C_{abcd}C^{abcd}|_{\mathcal{T}} = \frac{1024\pi^2}{3\gamma^4\Delta^2} + \mathcal{O}\left(\left(\frac{\ell_{\rm Pl}}{m}\right)^{\frac{2}{3}}\ln\frac{m}{\ell_{\rm Pl}}\right); \quad (4.15)$$

(iv) and, consequently, the Kretschmann scalar $K = R_{abcd}R^{abcd}$ has the asymptotic form

$$K|_{\mathcal{T}} = \frac{768\pi^2}{\gamma^4\Delta^2} + \mathcal{O}\left(\left(\frac{\ell_{\rm Pl}}{m}\right)^{\frac{2}{3}}\ln\frac{m}{\ell_{\rm Pl}}\right). \quad (4.16)$$

These expressions have two notable features. First, the area gap Δ appears in the denominator, bringing out the fact the finiteness of all upper bounds can be directly traced back to quantum geometry. Second, the leading terms are mass independent and their denominator is quadratic in $\gamma^2\Delta$ [which, by footnote 4, equals $\Delta^3/(48\pi^2\ell_{\rm Pl}^4)$]. However, the numerical coefficients vary. (The same pattern is encountered in LQC of the FLRW models.)

Note that these asymptotic forms refer to the transition surface $\mathcal{T}$. Since there is a precise sense in which the classical singularity is replaced by $\mathcal{T}$ in the effective theory, intuitively it is clear that these values would also be the upper bounds on curvature scalars of the effective metric throughout the spacetime region under consideration. However, since the expressions of these scalars at a general time are much more intricate, it is difficult to verify the validity of this expectation analytically. (For example, while the expression of the Kretschmann K scalar is simply
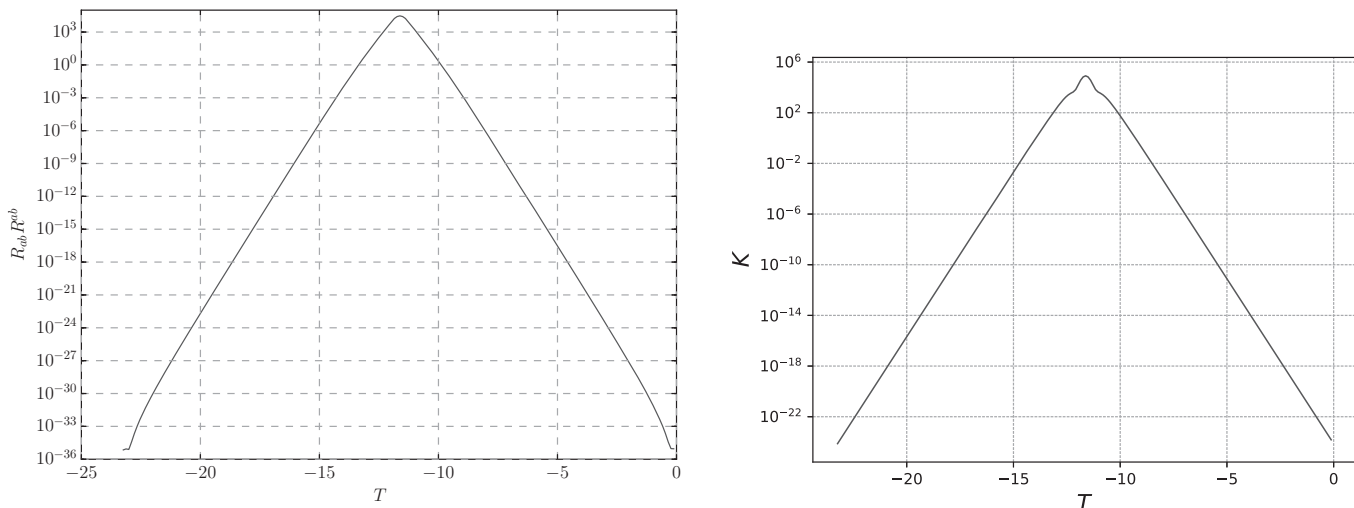
FIG. 1.   Time evolution of curvature scalars in the quantum corrected Schwarzschild interior for $m = 10^6$ (in Planck units). (The time parameter T is negative in the spacetime region under consideration and decreases as we move to the future.) The black hole–type horizon occurs to $T = 0$, the transition surface $\mathcal{T}$ lies at $T = -11.62$ and the white hole–type at $T = -23.24$. Spacetime region to the past of $\mathcal{T}$ is trapped and to the future of $\mathcal{T}$ is antitrapped. Curvature scalars are bounded throughout this evolution and attain their only maximum on $\mathcal{T}$ that replaces the classical singularity. Left panel: The invariant $R_{ab}R^{ab}$. The Ricci curvature is induced by quantum corrections and responsible for the singularity resolution. Although it is of Planck scale near $\mathcal{T}$, it decays rapidly away from $\mathcal{T}$ and is of the order of 10^{-35} in Planck units near the two horizons. Right panel: The Kretschmann scalar $R_{abcd}R^{abcd}$. It also has a single maximum at $\mathcal{T}$, decreases as we move away from $\mathcal{T}$ and is extremely close to the classical value $3/(4m^4) \approx 10^{-24}$ in Planck units near the two horizons. Thus, the ratio $R_{ab}R^{ab}/K_{\mathrm{class}}$ is very small, $\sim 10^{-13}$ near the horizon even when the black hole has as small a mass as $10^6 M_{\mathrm{Pl}}$ and it becomes much smaller for truly macroscopic black holes.

$48m^2/p_c^3$ in classical general relativity, it has more than twenty complicated terms in the effective theory.) Therefore, we carried out numerical evaluations for several values of the mass parameter $M = m/G$. Figures 1 and 2 illustrate the situation for $m = 10^6 \ell_{\mathrm{Pl}}$. The Ricci tensor R_{ab}, the energy density ρ and the effective pressures $\mathfrak{p}_x, \mathfrak{p}_\parallel$

are all zero in classical general relativity. But they acquire large Planck scale values near the transition surface $\mathcal{T}$ which, however, decay very rapidly as we move away from $\mathcal{T}$. Near the two horizons, their values are $\sim 10^{-20}$ or less, while $K^{1/2}$—the square-root of the Kretschmann scalar which has the same dimensions—is of the order
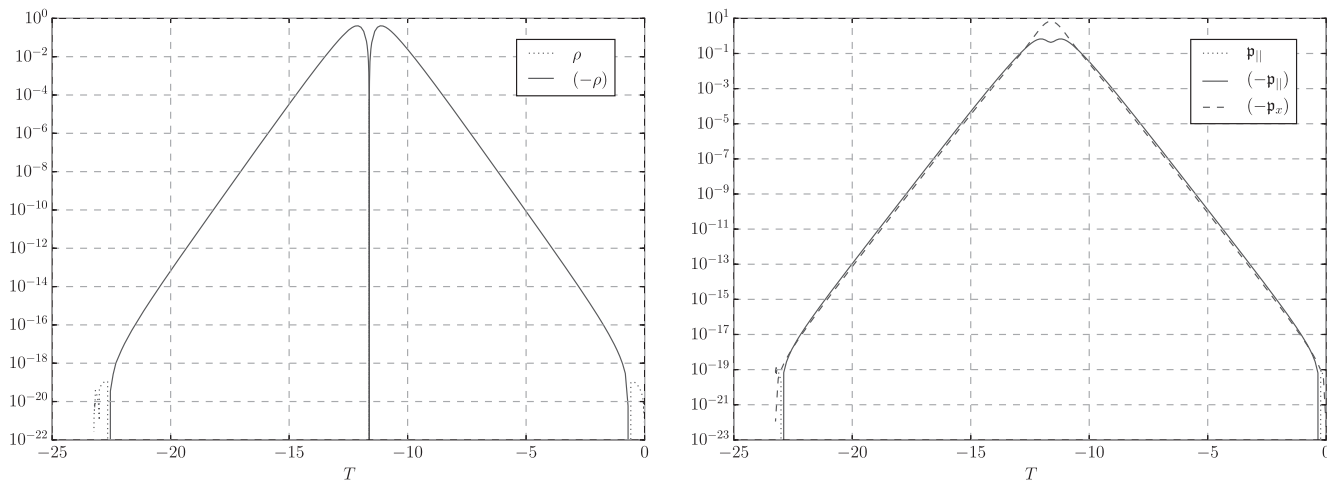

FIG. 2.   Time evolution in the quantum corrected Schwarzschild interior for the same mass as in Fig. 1 ($m = 10^6$). All quantities plotted are identically zero in classical general relativity and have their origin in quantum geometry. They attain their only maximum at the transition surface and decay rapidly away from $\mathcal{T}$. Left panel: energy density ρ is negative almost everywhere (solid line) in the interior region except in small neighborhoods of the two horizons (dotted lines). Right panel: radial pressure $\mathfrak{p}_x$ (dashed line) and tangential pressure $\mathfrak{p}_\parallel$ (solid line) are both negative almost everywhere in the interior region, but the tangential pressure $\mathfrak{p}_\parallel$ becomes positive in small neighborhoods of the two horizons (dotted lines).

10^{-12} there. Thus, the contribution of the Ricci tensor to the total curvature is completely negligible near the horizon already for black holes whose Schwarzschild radius is as small as $10^6 \ell_{Pl}$ and they become even more negligible for truly macroscopic black holes. Thus, just as in LQC, although the quantum geometry corrections are sufficiently large in the Planck regime to resolve the singularity, they decay rapidly as spacetime curvature becomes a few orders of magnitude smaller. In this precise sense, quantum gravity corrections play no role near horizons of large black holes in our model, contrary to what is sometimes suggested in other programs (see, e.g., [39]). Finally, Fig. 2 shows that ρ, $\mathfrak{p}_x$, $\mathfrak{p}_\parallel$ are all negative in a large neighborhood of $\mathcal{T}$, whence the strong energy condition is violated there, just as one would expect from the singularity resolution.

D. Comparison with prior LQG investigations

As mentioned in Sec. I, previous LQG investigations of the Schwarzschild interior using Kantowski-Sachs cosmology can be naturally divided into three classes. We will compare and contrast our strategy and results with those used in these three types of schemes. Some key differences predicted by various approaches are shown in the dynamics of p_c and p_b in Fig. 3.

1. μ_o-type approaches

Reference [37] used quantum kinematics that descends from full LQG and showed that the big-bang singularity in FLRW models is naturally resolved, thanks to the area gap in LQG. This strategy has since come to be known as the μ_o scheme. The underlying ideas were carried over to the analysis of the Schwarzschild singularity in Refs. [4,5]. The kinematical framework introduced in [4,37] and the idea of incorporating quantum gravity corrections to dynamics by representing curvature in terms of holonomies around 'elementary plaquettes' continue to be widely used in the analysis of cosmological and black hole singularities. However, subsequent investigations of detailed predictions brought out the fact that the specific implementation of this strategy in [4,5] has several important drawbacks (see, e.g., [10,21,28,40]). In this sense, while investigations like those in Refs. [4,37] served to open a fruitful avenue, they have to be suitably modified for physical viability.

In the Schwarzschild case, the situation can be summarized as follows. In Refs. [4,5,8], the new quantum parameters δ_b, δ_c are assumed to be constants: the 'area-gap argument' was used to set their values to

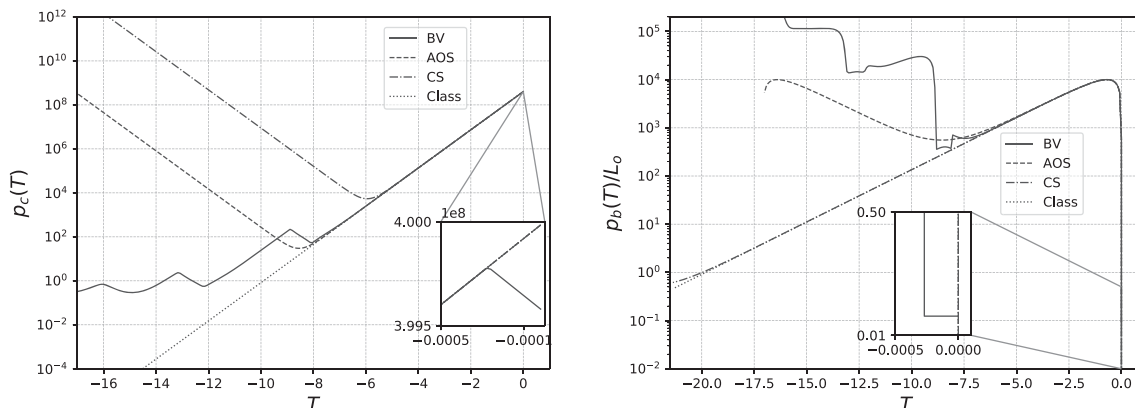$$\delta_b = \delta_c = 2\sqrt{3} =: \delta. \qquad (4.17)$$

FIG. 3. Comparison between the dynamical behavior of the triad components p_c and p_b in various LQG approaches for $m = 10^4$. In the effective spacetime geometry, transition surfaces $\mathcal{T}$ occur each time p_c undergoes a bounce. They separate trapped and antitrapped regions. (As in previous figures, the black hole–type horizon lies at $T = 0$ and T becomes more and more negative as time evolves.) The label "Class" refers to classical dynamics in which there is no bounce; the label "CS" refers to the generalized μ_o scheme [10] discussed in Sec. IV D 3; "AOS" refers to the dynamics in our approach discussed in Secs. III and IV A–IV C; and "BV" refers to dynamics in the $\bar{\mu}$-type scheme [6] discussed in Sec. IV D 2. Left panel: Evolution of p_c. In the classical theory p_c decreases steadily corresponding to the monotonic decrease in the radius of the round 2-spheres. In CS and AOS, it undergoes precisely one bounce, with trapped region to the past of the bounce and antitrapped to the future. In BV, it undergoes several bounces. The antitrapped region after the first bounce is very short lived. After the second bounce this $\bar{\mu}$ scheme cannot be trusted because its underlying assumptions are violated. Right panel: Evolution of p_b. This triad component does not play a direct role in determining the trapped and antitrapped regions. But it enters in the expression of the norm of the translational Killing field X^a and its vanishing signals the emergence of a black hole–or white hole–type horizon. The white hole–type horizon emerges much later in the CS approach [10] than in AOS reflecting the fact that there is a large mass amplification in the CS approach while there is no amplification in the AOS approach (in the large m limit). The BV approach [6] becomes unreliable after $T \sim -12$. The zooms shows another limitation of the BV approach: very near the black hole–type horizon, the BV dynamics deviates from the classical theory even though spacetime curvature is still small. The AOS dynamics is indistinguishable from classical dynamics near this horizon.

(More precisely, the fractional length of the link in the x direction was taken to be δ and the coordinate lengths in the θ and ϕ direction were taken to be δ.) Constancy of these parameters simplifies the analysis considerably and it is possible to obtain the explicit action of the Hamiltonian constraint operator on the kinematical Hilbert space. In the classical theory, p_c can be interpreted as an internal time. This choice is viable since (up to a factor of 4π) it determines the area of 2-spheres, which in the spacetime language equals τ^2. The form of the constraint operator is such that the quantum constraint equation can be thought of as providing an evolution along the 'internal time variable' provided by eigenvalues of $\hat{p}_c$. One can then verify that the singularity is absent in the quantum evolution.

To understand this prediction in detail, dynamics of this model was analyzed in detail in [10] using effective field equations.[9] The key result on singularity resolution holds also in the effective theory and, furthermore, one now has a detailed understanding of the quantum corrections to Einstein's equations that are responsible for this resolution. In particular, the area of the round 2-spheres—encoded in p_c—decreases to a minimum nonzero value and then increases again till one arrives at a white hole–type horizon. However, the analysis also revealed a key limitation of the way in which the main ideas are implemented in [4,5]. It turns out that physical quantities such as values of expansion and shear (of the normal to the homogeneous slices), as well as the minimum value of p_c depend on the value of L_o used to construct the fiducial cell $\mathcal{C}$. Another key observable is the radius of the white hole–type horizon that determines as the ADM mass in the corresponding asymptotic region. This too depends on L_o. Thus, while the qualitative features such as singularity resolution because of a transition surface and the subsequent emergence of antitrapped region are robust, quantitative predictions for spacetime geometry emerging from this dynamics can not be trusted because those numbers have no 'gauge-invariant' meaning. The origin of this L_o dependence can be traced back directly to the choice of δ_c in (4.17). Since the effective equations contain (trigonometric) functions of $c\delta_c$ and, as we saw in Sec. II, it is only c/L_o that is invariant under the rescaling $L_o \to \alpha L_o$ of the fiducial cell, constancy of δ_c implies that the solutions to effective equations can carry an L_o dependence.

Our systematic numerical investigation revealed another limitation that is more subtle but conceptually equally important. If δ_b, δ_c are assumed to be constant, then quantum effects can become important even in low curvature regime.

---

[9]Although the effective equations are yet to be systematically derived from the quantum evolution in this model, experience with anisotropic cosmological models [31] suggests that for macroscopic black holes they will approximate the exact evolution quite accurately if the quantum state is chosen to be sharply peaked along the classical dynamical trajectory initially, i.e., in the weak curvature region.

For large black holes, the Kretschmann scalar K at and near the black hole horizon is very small. Already for $m = 10^5$, we have $K = 7.5 \times 10^{-21}$ at the horizon. In this approach, the effective spacetime metric agrees with the classical metric to an excellent approximation till the curvature grows to $K \sim 10^{-19}$ but then coefficients of the two metrics start deviating and by the time the curvature becomes $K \sim 10^{-18}$ they are quite different from one another.

Remark: The μ_o-type approach is used also in [8] where, however, a deparametrization is carried out using the phase space variable c as the internal time and a quantum corrected effective description is obtained using an eikonal approximation. Qualitatively the results are similar to those of the effective description summarized above. In particular, p_c undergoes a bounce. In our terminology, the parameters δ_b, δ_c are set equal to a numerical value as in [4]. Therefore, the detailed predictions are again sensitive to the choice of L_o.

2. $\bar{\mu}$-type approaches

In FLRW models, limitations of the μ_o scheme were overcome through the so-called $\bar{\mu}$ scheme [28]. Soon thereafter, the technical ideas behind the $\bar{\mu}$ scheme were applied to the Schwarzschild interior in Refs. [6,7] in the framework of effective theories. The key difference from [4,5] is that δ_b, δ_c are no longer constants on the phase space: they are now phase space-functions

$$(\delta_b)^2 = \frac{\Delta}{p_c} \quad \text{and} \quad L_o^2(\delta_c)^2 = p_c \Delta \frac{L_o^2}{p_b^2}. \qquad (4.18)$$

(Note that, as needed, δ_b, $L_o\delta_c$ are invariant under the rescaling $L_0 \to \alpha L_o$ of the fiducial cell because p_b/L_o is invariant.) Since δ_c depends on both p_c and p_b, now the dynamical equations in the b, p_b sector no longer decouple from those in the c, p_c sector. As a consequence, it has not been possible to write down analytical solutions; all explorations of the Schwarzschild interior in this approach have, therefore, been numerical [6,7,20,21].

In FLRW models, while physical results can depend on choices of fiducial structures in the μ_o scheme, this is no longer the case in the $\bar{\mu}$ scheme [28]. Similarly, while quantum corrections can become important in low curvature regions in the μ_o scheme, this does not occur in the $\bar{\mu}$ scheme. Therefore, initially it was hoped that these limitations of [4,5] would be absent in [6,7]. This expectation was borne out in part: The dependence on fiducial structures is indeed removed. However, the effective theory still has the second problem: there can be large quantum corrections in the low curvature region near the black hole horizon. This can be most readily seen as follows. In the classical theory, since the spacelike $\tau = \text{const}$ surfaces become null in the limit $\tau \to 2m$, and in the Kantowski-Sachs model, the expansion and anisotropic shears are calculated using the unit timelike normal to the $\tau = \text{const}$

surfaces. Therefore, they diverge in the limit $\tau \to 0$ even though curvature at the horizon is very small for large black holes. The $\bar{\mu}$-type scheme does not distinguish between these harmless divergences and genuine singularities where spacetime curvature diverges. $\bar{\mu}$-type schemes trigger large quantum corrections that make expansion and shears finite [21] even at the horizon. Consequently, there are large departures from the classical theory very near the horizon. In terms of spacetime metric, our numerical evaluations show the same phenomenon in the dynamical behavior of b, p_b, both of which vanish classically at the horizon. In the phase space, the classical and the effective trajectories differ significantly from each other, but only when one is very close to the horizon.

Remark: Had we been interested in Kantowski-Sachs cosmologies rather than the Schwarzschild interior, we would introduce matter fields in the form of a perfect fluid. Then, in classical general relativity the horizon is replaced by a (pancake-type) curvature singularity. The large quantum corrections unleashed by the $\bar{\mu}$ scheme would then be physically appropriate.

If one moves away slightly from the horizon but remains in the low curvature region, the effective trajectories of the scheme proposed in Ref. [6] agree with the classical trajectories. When the curvature reaches Planck scale, p_c reaches a minimum and bounces, giving rise to a transition surface $\mathcal{T}$. (Interestingly, $\mathcal{T}$ emerges somewhat before it does in the scheme proposed in this paper, i.e., when the curvature is smaller.) As in Sec. II, to the past of $\mathcal{T}$ we have a trapped region and to the future an antitrapped region in which p_c increases. However, the later evolution is qualitatively different from that in Secs. IV B and IV C (see Fig. 3). Now, the untrapped region is very small because p_c undergoes *another* bounce and starts decreasing. Consequently, there is a new transition surface to the future of which we now have a trapped region. In this region, p_c decreases. But the model becomes self-inconsistent because very soon p_c has decreased so much that the round 2-spheres have an area smaller than Δ whence the required plaquette $\Box(\theta, \phi)$ cannot be fitted on the 2-sphere. That is, the requirements of the $\bar{\mu}$-scheme can no longer be implemented, whence its dynamical predictions cease to be meaningful. If one nonetheless continues the evolution as a mathematical exercise, one finds that the spacetime geometry asymptotically approaches that of the Nariai-type solution [6,11]. However, conceptually this last prediction is not meaningful because, strictly speaking, the $\bar{\mu}$ scheme stops being applicable long before this stage is reached. Physically, the scheme is not useful to explore the Schwarzschild interior because it sends the dynamical trajectory to phase space points where it ceases to be applicable. In this sense, it fails by its own criteria.

Remark: Whereas Ref. [6] considers vacuum Kantowski-Sachs spacetimes that are directly relevant for the analysis of Schwarzschild interior, Refs. [7,21] introduce matter sources. Similarly, in Refs. [9,11], Kantowski-Sachs models with cosmological constant were studied along with a parallel treatment of locally rotationally symmetric (LRS) Bianchi-III spacetimes. These analyses used the $\bar{\mu}$ prescription but their results are not directly relevant to the Schwarzschild interior studied here. Indeed, the focus there was to probe issues related to the Kantowski-Sachs cosmology such as whether the singularity is resolved for general matter fields, whether it is possible to single out preferred quantization schemes in these cosmologies, e.g., by requiring that expansion and shears remain bounded, and other issues that had not been studied in LQC.

3. Generalization of the μ_o-type approach allowing mass dependence

To improve upon this situation, one can make a different choice of the quantum parameters δ_b, δ_c [10,12]. Reference [10] modified the earlier μ_o-type prescription using dimensional considerations and made it free of choice of fiducial structures, while choices made in Ref. [12] were catered to obtain a symmetric bounce by phenomenologically modifying the scheme in Ref. [10]. These choices can be viewed as lying 'in between' the μ_o and $\bar{\mu}$ schemes because they ask that δ_b, δ_c be phase space functions that are constant along any given dynamical trajectory, but allow them to vary from one dynamical trajectory to another. Then, as we discussed in Sec. II B, the effective equations in the b, δ_b sector decouple from those in the c, δ_c sector and the solutions are given by (2.21)–(2.25).

Recall that under the rescaling $L_o \to \alpha L_o$, the connection component b is invariant but c changes via $c \to c/\alpha$. Since b and c enter the effective equations only via (trigonometric) functions of $b\delta_b$ and $c\delta_c$, to ensure cell independence of their solutions one needs to specify δ_b and $L_o\delta_c$ in a way that they do not make reference to fiducial structures. Since $m := \sin(\delta_c c)p_c/(\delta_c L_o \gamma)$ is a constant of motion [see (2.26)], using dimensional considerations δ_b, δ_c were set to

$$(\delta_b)^2 = \frac{\Delta}{(2m)^2} \quad \text{and} \quad L_o^2(\delta_c)^2 = \Delta. \quad (4.19)$$

Thus, as in the μ_o scheme, δ_c is constant on the entire phase space, but δ_b now depends on m and, thus, varies from one dynamical trajectory to another. Although the area gap Δ features in the expressions, the ansatz is motivated by phenomenological rather than fundamental considerations because one does not specify how the plaquettes $\Box(\theta, \phi), \Box(x, \theta), \Box(x, \phi)$ enclosing area Δ are to be chosen. Rather, the prescription (4.19) was made because it is the simplest one that is dimensionally consistent and meets the 'cell-independence' requirement.

Physical predictions of the effective dynamics resulting from this modified μ_o scheme have several attractive features [10]. First, by design they are all insensitive to the choice of L_o. Second, it again follows from (2.22) that

p_c has one and only one minimum. In the spacetime picture, this again implies that the extended effective spacetime is divided into a trapped and an antitrapped region, separated by the transition surface $\mathcal{T}$ (which corresponds to the absolute minimum of p_c). Third, the antitrapped region has a future boundary that corresponds to a white hole–type horizon. Finally, unlike in the $\bar{\mu}$ scheme, the expansion and shear grow unboundedly near the black hole horizon; for large black holes, the spacetime geometry near horizons is well approximated by general relativity. Thus, the spacetime picture is qualitatively similar to that in Secs. III, IV B and IV C.

However, there are two major differences. First, for large black holes, while the trapping surface $\mathcal{T}$ always emerges in the Planck regime in our approach, in this generalized μ_o scheme, it can emerge in low curvature regime. In fact, the curvature at $\mathcal{T}$ goes to zero in the limit $m \to \infty$. Thus, for astrophysical black holes very large quantum effects arise in low curvature regions. This feature can be qualitatively understood as follows. Equation (2.22) implies that at the transition surface $\mathcal{T}$, we have $p_c|_{\mathcal{T}} = m(\gamma L_o \delta_c)$. Since in this approach $L_o \delta_c = \sqrt{\Delta}$, we have: $p_c|_{\mathcal{T}} = (\gamma \sqrt{\Delta})m$. Now, in classical general relativity the Kretschmann scalar[10] is given by $K_{\text{cl}} = 48 m^2/p_c^3$. Therefore, at the bounce surface $K_{\text{cl}} = 48/(\gamma^3 \Delta^{3/2} m)$; it decreases as $1/m$. This dependence is borne out in numerical simulations.

Remark: The requirements of cell dependence and dimensional consistency criteria do restrict the choice of δ_b, δ_c, but they still leave considerable freedom because m^2/Δ is dimension free. Our proposal for δ_b, δ_c of Sec. IV A also satisfies these criteria. However, now the transition surface $\mathcal{T}$ always emerges in the Planck regime, and, furthermore, curvature scalars have an absolute, mass independent upper bounds. These features can also be understood using the same general considerations. As noted above, if δ_b, δ_c are Dirac observables, then at the transition surface p_c is given by $p_c|_{\mathcal{T}} = m(\gamma L_o \delta_c)$. In our choice (4.6), we have $L_o \delta_c = C m^{-1/3} \Delta^{2/3}$ where C is a dimensionless constant. Therefore, it follows that the classical Kretschmann scalar is now a Planck scale, mass independent constant: $K_{\text{cl}} = (48/\gamma^3 C^3 \Delta)$. While the Kretschmann scalar of the effective metric has a much more complicated form, as we showed in Sec. IV C, its leading term is also mass independent and of Planck scale for the macroscopic black holes we are interested in.

The second major difference between this generalized μ_o scheme and the one introduced in this paper is the

following. In our approach, the radius of the white hole–type horizon is the same as that of the initial black hole horizon in the large m limit. As we will see in Sec. V, this implies that the ADM mass in asymptotic region III associated with the white hole horizon agrees with that in the asymptotic region I associated with the initial black hole horizon:

$$m_{\text{WH}} = m_{\text{BH}} \left(1 + \mathcal{O}\left(\left(\frac{\ell_{\text{Pl}}}{m} \right)^{\frac{2}{3}} \ln\left(\frac{m}{\ell_{\text{Pl}}} \right) \right) \right). \quad (4.20)$$

In the generalized μ_o scheme, on the other hand, there is a tremendous mass amplification, approximately given by [10]

$$m_{\text{WH}} \approx (m_{\text{BH}}) \left(\frac{m_{\text{BH}}}{\ell_{\text{Pl}}} \right)^3. \quad (4.21)$$

For a solar mass black hole this would be an increase by a factor $\sim 10^{114}$! The physical origin of this huge increase has remained unclear.

Finally, Ref. [12] studied the possibility of removing the mass amplification within the broad idea of using a generalized μ_o-scheme but modifying the ansatz (4.19) to

$$(\delta_b)^2 = \alpha^2 \frac{\Delta}{(2m)^2} \quad \text{and} \quad L_o^2 (\delta_c)^2 = \beta^2 \Delta, \quad (4.22)$$

where α, β are dimensionless constants. Again, the approach is phenomenological in the sense that there is no prescription to choose the plaquettes that are to enclose the area Δ. Rather, the idea was to first stipulate conditions on α and β to reduce the freedom to a single constant and fix that remaining freedom by imposing the requirement that the mass amplification factor be 1. Three possibilities were explored: (i) $\beta = 1$; (ii) $\alpha = 1$ and (iii) $\alpha\beta = 1$. Because the final goal of arriving at the mass amplification factor of 1 is also realized in our approach in the large m limit, there is some similarity between the two. However, there are also differences. At the conceptual level, our choice (4.6) of Dirac observables δ_b, δ_c was arrived at by specifying the plaquettes. At a practical level, none of the three choices of [12] is compatible with our choice (4.6). For example, with choices (i) and (iii), the forms of δ_b, δ_c are not known analytically even for the large m, while in our approach they are given simply by (4.6). For choice (ii), the asymptotic forms for large m are given in [12], and they imply $p_c|_{\mathcal{T}} \approx (\gamma \Delta^2)/m^2$ at the transition surface. Hence now the classical expression of the Kretschmann scalar $K_{\text{cl}} = 48 m^2/p_c^3 = C m^8/\Delta^4$ (where C is a dimensionless constant) grows unbounded with m. In our approach, it has a mass independent upper bound.

V. QUANTUM EXTENDED KRUSKAL SPACETIME

This section is divided into two parts. In the first, we introduce a new approach to obtain the quantum corrected

---

[10]In the effective theory, the expression of the Kretschmann scalar is much more complicated. However, for large m, the effective trajectory is well approximated by the classical one until it reaches close to the p_c-bounce. (For example, even for a rather low value of mass, $m = 10^5$, the transition surface emerges at $T = -7.1$ while the two trajectories are indistinguishable between $T = 0$ and $T = -6$.) Therefore, the classical expression of K provides a very good approximation to the actual value.

effective metric in the exterior region between the horizon and infinity using LQG techniques as in Sec. II. In the second, we show that the effective metric in the interior and the exterior regions match seamlessly and investigate properties of the resulting quantum extension of Kruskal spacetime.

A. The Schwarzschild exterior

1. Phase space for the exterior region

As we saw in Sec. II, a finite dimensional phase space can be constructed for the interior region using the fact that it is foliated by spatially homogeneous spacelike 3-manifolds Σ. Since phase spaces are normally constructed using Cauchy surfaces and since none in the exterior region are homogeneous, Hamiltonian descriptions of the exterior have been qualitatively different. On the one hand, they are much more complicated because the inhomogeneity of the spatial metric makes these standard phase spaces infinite dimensional. On the other hand, since the exterior is static, discussion of dynamics is somewhat vacuous.

Our new observation that changes this status quo is rather simple. While the exterior cannot be foliated by spacelike homogeneous surfaces, it is foliated by timelike homogeneous surfaces ($r = $ const in the standard Schwarzschild coordinates) whose isometry group is again $R \times SO(3)$. Therefore, the phase space based on these slices is again finite dimensional and there is now nontrivial dynamics as one evolves from one timelike homogeneous surface to another in the radial direction. While this is somewhat counter-intuitive at first because this evolution is in a spacelike direction, there is nothing unusual about the setup from the Hamiltonian perspective even for full general relativity: One again has constraint equations on the canonical variables, and 'dynamics' is again be generated by a Hamiltonian constraint. Indeed, such evolutions in spatial directions are already used extensively in LQG in the context of Euclidean/Riemannian frameworks. Of course, considerable work is needed to extend the LQG framework to cover this situation and it is far from being clear that all potential problems can be handled satisfactorily.[11]

In the Kruskal spacetime now under consideration, not only will the 'dynamics' again be generated by a

Hamiltonian constraint, but the evolution equations will again be ODEs as in Sec. II. The only difference from the situation in Sec. II is that now the intrinsic metric q_{ab} has signature $-, +, +$ (rather than $+, +, +$) and, therefore, the internal space for the gravitational connection and triads also has signature $-, +, +$ (rather than $+, +, +$). This means that the gauge group of internal rotations for the gravitational connection is now SU(1, 1) [rather than SU(2)]. While a convenient basis in the Lie algebra of SU(2) is given by τ_i used in Eqs. (2.6) and (2.7), for SU (1, 1) it is given by $\tilde{\tau}_i$, related to τ_i via:

$$\tilde{\tau}_1 = i\tau_1, \qquad \tilde{\tau}_2 = i\tau_2, \qquad \tilde{\tau}_3 = \tau_3. \qquad (5.1)$$

Keeping this difference in mind, we can simply follow the procedure used in Sec. II step by step. Let us, therefore, consider a 3-manifold $\tilde{\Sigma}$ again with topology $\mathbb{R} \times \mathbb{S}^2$ and introduce on it a fiducial metric

$$\mathring{\tilde{q}}_{ab}\mathrm{d}x^a\mathrm{d}x^b = -\mathrm{d}x^2 + r_o^2(\mathrm{d}\theta^2 + \sin^2\mathrm{d}\phi^2) \qquad (5.2)$$

where, again, $x \in (-\infty, \infty)$, θ and ϕ are 2-sphere coordinates and r_o is a constant. (Note that x is now a timelike coordinate, $\partial/\partial x$ being the time translation Killing field in the exterior region.) Then, thanks to the underlying homogeneity we can solve the spatial diffeomorphism constraint and perform a partial gauge fixing to satisfy the Gauss constraint. As a result, the gravitational connection and the conjugate densitized triad can be expressed as in equations (2.6) and (2.7) simply by replacing τ_i by $\tilde{\tau}_i$ and using the relation (5.1) between the two:

$$A_a^i\tilde{\tau}_i\mathrm{d}x^a = \frac{\tilde{c}}{L_o}\tau_3\mathrm{d}x + i\tilde{b}\tau_2\mathrm{d}\theta - i\tilde{b}\tau_1\sin\theta\mathrm{d}\phi + \tau_3\cos\theta\mathrm{d}\phi,$$

$$(5.3)$$

and

$$E_i^a\tilde{\tau}^i\partial_a = \tilde{p}_c\tau_3\sin\theta\partial_x + \frac{i\tilde{p}_b}{L_o}\tau_2\sin\theta\partial_\theta - \frac{i\tilde{p}_b}{L_o}\tau_1\partial_\phi. \quad (5.4)$$

Comparing these equations with (2.6) and (2.7), it is clear that the phase space for the exterior region can be obtained simply by making the substitutions

$$b \to i\tilde{b}, \quad p_b \to i\tilde{p}_b; \qquad c \to \tilde{c}, \quad p_c \to \tilde{p}_c \qquad (5.5)$$

in equations of Sec. II. In particular, the Poisson brackets are now given by:

$$\{\tilde{c}, \tilde{p}_c\} = 2G\gamma, \qquad \{\tilde{b}, \tilde{p}_b\} = -G\gamma. \qquad (5.6)$$

---

2. Classical dynamics of the exterior region

Let us now turn to dynamics. From spacetime perspective, since the radial coordinate τ satisfies $\tau > 2m$ in the exterior region, the Hamiltonian dynamics simply 'evolves' the geometry in radial directions filling out the exterior region $2m < \tau < \infty$, starting from the data at some $\tau_0 > 2m$. However, it is instructive to examine this evolution as a dynamical trajectory in phase space as a prelude to the investigation of the effective dynamics.

We begin by writing the Hamiltonian constraint for the exterior region, obtained simply by using the substitutions (5.5) in (2.11):

$$\tilde{H}_{\text{cl}}[\tilde{N}_{\text{cl}}] = -\frac{1}{2G\gamma}\left(2\tilde{c}\,\tilde{p}_c + \left(-\tilde{b} + \frac{\gamma^2}{\tilde{b}}\right)\tilde{p}_b\right). \quad (5.7)$$

As one would expect, evolution equations for connection and triad variables obtained using (5.6) and (5.7) are the same as those that result if one uses the substitutions (5.5) in (2.12) and (2.13). One can easily integrate these equations and use (5.7) to simplify the solutions. The result is:

$$\tilde{b}(T_{\text{cl}}) = \pm\gamma(1 - e^{-T_{\text{cl}}})^{1/2}, \qquad \tilde{c}(T_{\text{cl}}) = \tilde{c}_o e^{-2T_{\text{cl}}}, \quad (5.8)$$

and

$$\tilde{p}_b(T_{\text{cl}}) = \tilde{p}_b^{(o)} e^{T_{\text{cl}}}(1 - e^{-T_{\text{cl}}})^{1/2}, \qquad \tilde{p}_c(T_{\text{cl}}) = \tilde{p}_c^{(o)} e^{2T_{\text{cl}}}, \quad (5.9)$$

where T_{cl} is the affine parameter along the Hamiltonian vector field generated by (5.7). The form of the solutions (5.8) and (5.9) immediately implies that $\tilde{c}\tilde{p}_c/(L_o\gamma)$ is a Dirac observable, i.e., it is a constant of motion. As we will see, in the spacetime metric associated with any dynamical trajectory, it again coincides with $m = GM$.

As in Sec. II A, we have fixed one of the integration constants so that the black hole horizon lies at $T_{\text{cl}} = 0$ in the spacetime picture. The remaining integration constants $\tilde{c}_o$, $\tilde{p}_b^{(o)}$ and $\tilde{p}_c^{(o)}$ can also be fixed as in Sec. II A to match the phase space variables with the corresponding spacetime geometry in the Schwarzschild exterior:

$$d\tilde{s}^2 = -\left(1 - \frac{2m}{\tau}\right)dx^2 + \left(1 - \frac{2m}{\tau}\right)^{-1}d\tau^2 + \tau^2(d\theta^2 + \sin^2\theta d\phi^2). \quad (5.10)$$

To set this correspondence, we first note that for any choice of the radial coordinate τ and the associated "lapse-squared" $\tilde{N}_\tau^2$, each point in the phase space defines a spacetime metric admitting a foliation by homogeneous timelike slices:

$$\tilde{g}_{ab}dx^a dx^b \equiv d\tilde{s}^2 = -\frac{\tilde{p}_b^2}{|\tilde{p}_c|L_o^2}dx^2 - \tilde{N}_\tau^2 d\tau^2 + |\tilde{p}_c|(d\theta^2 + \sin^2\theta d\phi^2). \quad (5.11)$$

(See Eq. (2.8). As we will see below, $\tilde{N}_\tau^2$ is negative, reflecting the fact that τ is a spacelike rather than a timelike coordinate.) Our solutions (5.8) and (5.9) are written for a specific choice T_{cl} of the radial coordinate in the exterior. As in Sec. II A, the transformation relating T_{cl} to the radial coordinate τ in (5.10) is: $\tau := 2me^{T_{\text{cl}}}$. With this information at hand, we can now use (5.8) and (5.9) in (5.11) and set up the desired dictionary by comparing the resulting expression with (5.10). Comparing the first and the last terms in these two expressions of the metric we obtain $|\tilde{p}_c| = \tau^2$ and $\tilde{p}_b^2 = L_o^2(1 - \frac{2m}{\tau})\tau^2$. With this choice of τ, the lapse takes the form $\tilde{N}_\tau^2 = -(1 - \frac{2m}{\tau})^{-1}$. Therefore, the remaining constants are given by: $\tilde{c}_o = \gamma L_o/4m$; $\tilde{p}_b^{(o)} = 2mL_0$; $\tilde{p}_c^{(o)} = 4m^2$. As in footnote 5, the more familiar Schwarzschild form is obtained by the obvious substitutions $x \to t$ and $\tau \to r$.

Finally we note that at the horizon we have $\tau = 2m$, whence as in the interior solution T_{cl} vanishes there and so do $\tilde{p}_b$ and $\tilde{b}$. Thus, in the phase space picture the horizon is characterized by the same conditions in both interior and exterior regions. We will see in Sec. V B 1 that the matching is seamless both in the phase space and spacetime pictures.

3. Effective dynamics of the exterior region

Let us now turn to effective dynamics on the phase space of Sec. V A 1 associated with the exterior region. We can now just follow the analysis of Sec. II B step by step. Substitutions (5.5) imply that the effective Hamiltonian constraint is given by:

$$\tilde{H}_{\text{eff}}[\tilde{N}] = -\frac{1}{2G\gamma}\left[2\frac{\sin(\delta_{\tilde{c}}\tilde{c})}{\delta_{\tilde{c}}}|\tilde{p}_c| + \left(-\frac{\sinh(\delta_{\tilde{b}}\tilde{b})}{\delta_{\tilde{b}}} + \frac{\gamma^2\delta_{\tilde{b}}}{\sinh(\delta_{\tilde{b}}\tilde{b})}\right)\tilde{p}_b\right]. \quad (5.12)$$

where $\delta_{\tilde{b}} = \delta_b$, $\delta_{\tilde{c}} = \delta_c$ continue to be given by (4.6). Thus, the same principle determines these quantum parameters both in the interior and the exterior. Note that the expression on the right side now involves trigonometric functions of $\delta_{\tilde{c}}\tilde{c}$ but hyperbolic functions of $\delta_{\tilde{b}}\tilde{b}$, reflecting the fact that the x direction is now timelike rather than spacelike while θ, ϕ directions continue to be spacelike. One can obtain the equations of motion using this Hamiltonian constraint and Poisson brackets (5.6) and find their solutions.

As one would expect, the solutions are the same as those resulting from substitutions (5.5) in the interior solution (2.21)–(2.25):

$$\tan\left(\frac{\delta_{\tilde{c}}\tilde{c}(T)}{2}\right) = \mp\frac{\gamma L_o \delta_{\tilde{c}}}{8m}e^{-2T}, \qquad (5.13)$$

$$\tilde{p}_c(T) = 4m^2\left(e^{2T} + \frac{\gamma^2 L_o^2 \delta_{\tilde{c}}^2}{64m^2}e^{-2T}\right), \qquad (5.14)$$

$$\cosh(\delta_{\tilde{b}}\tilde{b}(T)) = \tilde{b}_o \tanh\left(\frac{1}{2}\left(\tilde{b}_o T + 2\tanh^{-1}\left(\frac{1}{\tilde{b}_o}\right)\right)\right), \qquad (5.15)$$

where

$$\tilde{b}_o = (1 + \gamma^2\delta_{\tilde{b}}^2)^{1/2}, \qquad (5.16)$$

and,

$$\tilde{p}_b(T) = -2\frac{\sin(\delta_{\tilde{c}}\tilde{c}(T))}{\delta_{\tilde{c}}}\frac{\sinh(\delta_{\tilde{b}}\tilde{b}(T))}{\delta_{\tilde{b}}}\frac{|\tilde{p}_c(T)|}{\gamma^2 - \frac{\sinh^2(\delta_{\tilde{b}}\tilde{b}(T))}{\delta_{\tilde{b}}^2}}, \qquad (5.17)$$

where T is now the affine parameter along the Hamiltonian vector field generated by $\tilde{H}_{\text{eff}}[\tilde{N}]$. Note that, just as the b, p_b and c, p_c sectors decouple dynamically in the Schwarzschild interior, the $\tilde{b}, \tilde{p}_b$ and $\tilde{c}, \tilde{p}_c$ sectors also decouple in the exterior. The form of solutions in the $\tilde{c}, \tilde{p}_c$ sector is the same as that in the c, p_c sector, while in the $\tilde{b}, \tilde{p}_b$ sector, up to some changes in signs, trigonometric functions [such as $\sin(\delta_b b)$] are replaced by hyperbolic functions [such as $\sinh(\delta_{\tilde{b}}\tilde{b})$]. Because of the agreement of dynamics in the $\tilde{c}, \tilde{p}_c$ and c, p_c sectors, $\sin(\delta_{\tilde{c}}\tilde{c})\tilde{p}_c/(\delta_{\tilde{c}}L_o\gamma)$ continues to be a Dirac observable which in the classical regime has the interpretation of $m = GM$ of the black hole. Since our effective theory agrees with the classical theory in the low curvature region near the black hole horizon and since Dirac observables are constants of motion, as in Sec. II B, we will again denote it by m.

Finally, one can pass from the phase space to the spacetime description following the same procedure as in the classical theory, sketched in Sec. V A 2. The spacetime metric $\tilde{g}_{ab}$ is of the form (5.11)

$$\tilde{g}_{ab}dx^a dx^b = -\frac{\tilde{p}_b^2}{|\tilde{p}_c|L_o^2}dx^2 + \frac{\gamma^2|\tilde{p}_c|\delta_{\tilde{b}}^2}{\sinh^2(\delta_{\tilde{b}}\tilde{b})}dT^2$$
$$+ |\tilde{p}_c|(d\theta^2 + \sin^2\theta d\phi^2). \qquad (5.18)$$

since $\tilde{N}^2$ now has the form

$$\tilde{N}^2 = -\frac{\gamma^2|\tilde{p}_c|\delta_{\tilde{b}}^2}{\sinh^2(\delta_{\tilde{b}}\tilde{b})}. \qquad (5.19)$$

Explicit expressions of $\tilde{p}_c, \tilde{p}_b$ are given by (5.14) and (5.17).

B. Properties of the quantum extension of the Kruskal spacetime

From the Hamiltonian perspective, we have two distinct phase spaces, one spanned by $b, p_b; c, p_c$ and another by $\tilde{b}, \tilde{p}_b; \tilde{c}, \tilde{p}_c$, with Poisson brackets given by (2.5) and (5.6). Dynamics is generated by distinct Hamiltonian constraints—(2.11) and (5.7) in the classical theory and (2.18) and (5.12) in the effective theory. Nonetheless, as we show in Sec. V B 1 the spacetime geometries defined in the exterior and interior regions match smoothly across horizons. In Sec. V B 2, we investigate properties of the resulting quantum extension of the Kruskal spacetime.

1. Matching of interior and exterior geometries

Let us begin with the classical theory where the situation is straightforward. Dynamical trajectories in the interior phase space correspond to time $T_{\text{cl}} < 0$ while those in the exterior phase space correspond to $T_{\text{cl}} > 0$. In the spacetime interpretation, the $T_{\text{cl}} = 0$ surface is excluded in both descriptions since it is null. However, one can regard it as a limit of spacelike $T_{\text{cl}} = \text{const} < 0$ surfaces in the interior region and timelike $T_{\text{cl}} = \text{const} > 0$ surfaces in the exterior region and in both regions the limit represents a black hole–type horizon. Therefore, we can ask whether the geometry is smooth across this horizon. The triad variables are given, respectively, by

$$T_{\text{cl}} < 0: \quad p_b(T_{\text{cl}}) = p_b^{(o)}e^{T_{\text{cl}}}(e^{-T_{\text{cl}}} - 1)^{1/2},$$
$$p_c(T_{\text{cl}}) = p_c^{(o)}e^{2T_{\text{cl}}} \qquad (5.20)$$

and

$$T_{\text{cl}} > 0: \quad \tilde{p}_b(T_{\text{cl}}) = \tilde{p}_b^{(o)}e^{T_{\text{cl}}}(1 - e^{-T_{\text{cl}}})^{1/2},$$
$$\tilde{p}_c(T_{\text{cl}}) = \tilde{p}_c^{(o)}e^{2T_{\text{cl}}}, \qquad (5.21)$$

where $p_b^o = \tilde{p}_b^o = 2mL_0$ and $p_c^o = \tilde{p}_c^o = 4m^2$. Therefore, it is evident that the triad variables are smooth across the boundary $T_{\text{cl}} = 0$. Thus, the dynamical trajectory in the Schwarzschild interior can be joined smoothly with that in the exterior provided, of course, they both correspond to the same mass.

As one would expect, the situation for the spacetime metric is a bit more complicated simply because the constant T_{cl} surfaces are spacelike for $T_{\text{cl}} < 0$, timelike for $T_{\text{cl}} > 0$ and null at $T_{\text{cl}} = 0$. So, we have:

$$T_{\rm cl} < 0: \quad g_{ab}{\rm d}x^a{\rm d}x^b = -\frac{4m^2 e^{2T_{\rm cl}}}{(e^{-T_{\rm cl}} - 1)}{\rm d}T_{\rm cl}^2 + (e^{-T_{\rm cl}} - 1){\rm d}x^2 + 4m^2 e^{2T_{\rm cl}}({\rm d}\theta^2 + \sin^2\theta{\rm d}\phi^2)$$

$$T_{\rm cl} > 0: \quad \tilde{g}_{ab}{\rm d}x^a{\rm d}x^b = -(1 - e^{-T_{\rm cl}}){\rm d}x^2 + \frac{4m^2 e^{2T_{\rm cl}}}{(1 - e^{-T_{\rm cl}})}{\rm d}T_{\rm cl}^2 + 4m^2 e^{2T_{\rm cl}}({\rm d}\theta^2 + \sin^2\theta{\rm d}\phi^2), \tag{5.22}$$

where we have used the explicit form of the lapse $N_{\rm cl}^2$ and $\tilde{N}_{\rm cl}^2$ in the interior and the exterior regions [see Eq. (2.10)].

In both regions, the 4-metric is ill defined in the limit $T_{\rm cl} \to 0$. However, this is the standard coordinate singularity; spacetime geometry is in fact smooth there. As is well known, because the 2-sphere metric is smooth and non-degenerate at $T_{\rm cl} = 0$ and the determinant $g_{xx}g_{T_{\rm cl}T_{\rm cl}}$ of the 2-metric in the x-$T_{\rm cl}$ plane is smooth and nonvanishing there, one can introduce the standard Eddington-Finkelstein coordinates to show explicitly that the 4-metric is manifestly smooth across the horizon $T_{\rm cl} = 0$. This statement in terms of spacetime geometry is trivial. For the effective theory discussed below, the important observation is that smoothness of spacetime geometry across the horizon is guaranteed by the following properties of the dynamical trajectories in the phase space: at $T_{\rm cl} = 0$, (1) the pairs p_b, $\tilde{p}_b$ and p_c, $\tilde{p}_c$ admit smooth limits; (2) $N_{\rm cl}^2 = -\tilde{N}_{\rm cl}^2$, reflecting the fact that while $N_{\rm cl}^2$ refers to time-evolution in the interior region, $\tilde{N}_{\rm cl}^2$ refers to radial evolution in the exterior region; and, (3) $(N_{\rm cl}^2 p_b^2)/(p_c L_o^2)$ in the interior and its counterpart $(-\tilde{N}_{\rm cl}^2 \tilde{p}_b^2)/(|\tilde{p}_c| L_o^2)$ in the exterior are smooth, nonzero and equal. (Each of these quantities is the determinant of the 2-metric in the x-$T_{\rm cl}$ plane).

We will now show that these properties continue to hold also in the effective description. The expressions of triads along dynamical trajectories in the phase space are:

$$T < 0: \quad p_c(T) = 4m^2\left(e^{2T} + \frac{\gamma^2 L_o^2 \delta_c^2}{64m^2}e^{-2T}\right),$$

$$p_b(T) = -2mL_o\frac{\sin(\delta_b b(T))}{\delta_b}\frac{1}{\frac{\sin^2(\delta_b b(T))}{\delta_b^2} + \gamma^2};$$

$$\tag{5.23}$$

and

$$T > 0: \quad \tilde{p}_c(T) = 4m^2\left(e^{2T} + \frac{\gamma^2 L_o^2 \delta_{\tilde{c}}^2}{64m^2}e^{-2T}\right),$$

$$\tilde{p}_b(T) = -2mL_o\frac{\sinh(\delta_{\tilde{b}}\tilde{b}(T))}{\delta_{\tilde{b}}}\frac{1}{\gamma^2 - \frac{\sinh^2(\delta_{\tilde{b}}\tilde{b}(T))}{\delta_{\tilde{b}}^2}},$$

$$\tag{5.24}$$

where we have simplified the expressions of $p_b(T)$ and $\tilde{p}_b(T)$ using the form of the Dirac observable $m = (\sin\delta_c c)p_c/(\delta_c L_o\gamma) = (\sin\delta_{\tilde{c}}\tilde{c})\tilde{p}_c/(\delta_{\tilde{c}} L_o\gamma)$. Note that for matching the exterior and interior geometries, we are

interested in pairs of trajectories in the interior and exterior phase space with the same value of m. On these pairs, at $T = 0$ we have: $p_c = \tilde{p}_c = 4m^2(1 + \frac{\gamma^2 L_o^2\delta_c^2}{64m^2})$ and $p_b/L_o = \tilde{p}_b/L_o = 0$. Thus, the values of the triad variables match at $T = 0$ and by Taylor expanding them one can check that the matching is smooth. Therefore, condition (1) above is satisfied. Equations (2.17) and (5.19) imply that condition (2) is also satisfied. Finally, at $T = 0$ we have: $(N^2 p_b^2)/(p_c L_o^2) = (-\tilde{N}^2 \tilde{p}_b^2)/(|\tilde{p}_c| L_o^2) = 4m^2$ (which, incidentally is exactly the same as in the classical theory). Thus, condition (3) is also satisfied.

Let us conclude with a summary of the situation in the effective theory. We have separate, four-dimensional phase spaces describing the exterior and interior Schwarzschild geometries, depicted in Fig. 4 by region I and the black hole region B attached to it. They are coordinatized, respectively, by pairs $\tilde{b}, \tilde{p}_b; \tilde{c}, \tilde{p}_c$ with Poisson brackets (5.6), and pairs $b, p_b; c, p_c$, with Poisson brackets (2.5). Dynamics is governed by the Hamiltonian constraints (5.12) and (2.18) respectively. We identified a Dirac observable m in each phase space. The parameter T along trajectories $\tilde{b}(T)$, $\tilde{p}_b(T); \tilde{c}(T), \tilde{p}_c(T)$ in the exterior phase space has positive values and along trajectories $b(T), p_b(T); c(T), p_c(T)$ in the interior phase space takes negative values. Trajectories labeled by the same value of the Dirac observable m can be joined smoothly at $T = 0$. In the spacetime language, the (limiting) point $T = 0$ along each trajectory represents the black hole horizon. The coefficients in the spacetime metric become singular in the Schwarzschild-like coordinates (T, x), just as they do in the classical theory. However, the effective metric is smooth across the horizon. The metric coefficients are such that the determinant of the effective 4-metric remains smooth and nonzero across $T = 0$ whence, as in the classical theory, one can introduce new Eddington-Finkelstein–type coordinates to show that the effective geometry is manifestly smooth in the entire region I ∪ B ∪ W of Fig. 4, which encompasses the asymptotic region I as well as the black and white hole regions B and W that are joined at the transition surface $\mathcal{T}$. For the macroscopic black holes considered in this paper, the asymptotic region I is 'tame' as in the classical theory. However, the interior region B ∪ W includes Planck scale curvature where quantum geometry effects resolve the singularity.

2. Properties of the quantum extension

The procedure introduced in Sec. VA can be used again at the left boundary of the black hole region B to extend the
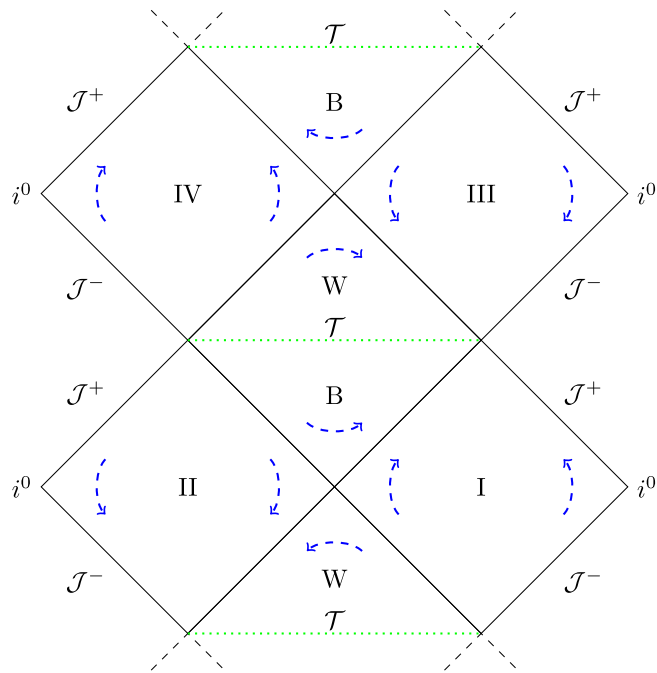
FIG. 4. The Penrose digram of the extended Kruskal spacetime. In Secs. III and IV, we began with the region B in the central diamond corresponding to the standard Schwarzschild trapped region. In the classical theory, spacetime ends at a horizontal line due to curvature singularity. In the effective geometry, the singularity is replaced by a transition surface $\mathcal{T}$ where $\dot{p}_c$ vanishes. The extended region has an antitrapped region labeled "W." Thus, quantum geometry provides a region bounded to the past by a black hole–type horizon and to the future by a white hole–type region. Effective metric for asymptotic regions I, II, III and IV is introduced in Sec. V A 3. Section V B 1 shows that it joins on smoothly to the geometry in the trapped and antitrapped regions B and W. As indicated by dashed lines, the same procedure continues the spacetime to new trapped and anti-trapped and asymptotic regions to the past and future. Arrows denote trajectories of the translational (or static) Killing field $X^a \partial_a = \partial_x$ in various regions.

effective spacetime to the asymptotic region II. Similarly, the procedure can be used at the future boundaries of the white hole region W to join the spacetime smoothly to asymptotic regions III and IV. These regions have future boundaries representing black hole–type horizons and so we can again repeat the procedure and extend the spacetime to future. Thus, the procedure provides a quantum extension of the Kruskal spacetime, where the effective spacetime metric is everywhere smooth and curvature invariants are uniformly bounded. The full extension has infinitely many asymptotic, trapped and antitrapped regions. This structure is shown in Fig. 4.

We will now discuss salient features of this quantum extension of Kruskal spacetime.

(i) Effective versus classical geometry: In the interior region, the effective geometry is very different from the classical one because quantum geometry

corrections to Einstein's equations become crucial. As we saw in Sec. IV B, these corrections can be regarded as providing an effective stress-energy tensor that violates the strong energy condition in the Planck regime, leading to singularity resolution. But we also saw that in the low curvature region near horizons, these quantum corrections become negligible and Einstein's equations provide an excellent approximation to the effective equations (Fig. 2).

What is the situation in the exterior region? Since the effective theory includes $\hbar$-dependent quantum corrections, effective metric never agrees completely with the classical Schwarzschild metric no matter how far one recedes from the horizon (just as general relativistic corrections to Newtonian theory are never zero for any physical system). However, quantum corrections are again negligible already at the horizon of macroscopic black holes and become even smaller rapidly in the asymptotic region. For concreteness, let us consider classical and effective solutions for $m = 10^4 M_{\mathrm{Pl}}$ and examine the differences in the two spacetime geometries in the asymptotic region I. Using MATHEMATICA, one finds the following illustrative numbers: (i) As Eqs. (5.9) and (5.14) show the horizon radius of the effective solution is slightly larger than that in the classical theory. The relative difference is only $\sim 10^{-15}$ and the corrections fall off as $m^{-8/3}$. So, for a solar mass black hole, the relative difference in the horizon radius is $\sim 10^{-106}$! (ii) In the classical theory, the Ricci tensor is identically zero. In the effective theory, at the horizon the square of the Ricci scalar of the effective metric is given by $R^2_{\mathrm{eff}} \approx 9.4 \times 10^{-25}$ in Planck units (for $m = 10^4$). It increases slightly as one recedes from the horizon and reaches a maximum of $(R^2)^{\mathrm{max}}_{\mathrm{eff}} \approx 1.2 \times 10^{-24}$ at $T \approx 0.13$ and then decays rapidly to zero. (Recall that the horizon corresponds to $T = 0$; in terms of the radial coordinate r, R^2_{eff} reaches its maximum at $\approx 1.14 r_{\mathrm{hor}}$.) More generally, $(R^2)^{\mathrm{max}}_{\mathrm{eff}} \sim 10^{-8} (\ell_{\mathrm{Pl}}/m)^4$. These are measures of absolute smallness of $(R^2)^{\mathrm{max}}_{\mathrm{eff}}$. Since the classical Kretschmann scalar at the horizon is $K_{\mathrm{cl}} \approx 7.5 \times 10^{-17}$, the relative smallness of the departure from Einstein's equations is $R^2_{\mathrm{eff}}/K_{\mathrm{cl}} \approx 10^{-8}$ at the horizon. (iii) One can also consider the square of the Ricci tensor of the effective metric. At the horizon it is $[R_{ab}R^{ab}]_{\mathrm{eff}} \approx 4.7 \times 10^{-25}$ and it decays rapidly in the asymptotic region (again for $m = 10^4 M_{\mathrm{Pl}}$). Thus, for macroscopic black holes, the Schwarzschild solution is an excellent approximation to the effective spacetime metric throughout region I and the approximation rapidly improves as one moves to the asymptotic region. Therefore, in this approach, large quantum

corrections outside the horizons of macroscopic black holes envisaged in some approaches (see, e.g., [39]) do not arise.

(ii) Nonamplification of mass: The approach most closely related to ours is the 'generalized μ_o-scheme' introduced and analyzed in detail in [10]. That investigation explored the effective geometry only in the interior region depicted by the central diamond B ∪ W in Fig. 4. A key feature of that effective geometry is that the radius r_W of the white hole–type horizon is very large compared the radius r_B of the black hole–type horizon in the diamond, growing as $r_W \approx r_B (r_B/\ell_{Pl})^3$. So if we start with $r_B = 3$ km–the Schwarzschild radius of a solar mass black hole–we have $r_W \approx 10^{93}$ Gpc! This effect was interpreted as quantum gravity induced mass inflation [see Eq. (4.21)]. However, the physical origin of this mass inflation has remained unclear.

In our approach, by contrast, the ratio of the two radii is very close to 1 for macroscopic black holes:

$$\frac{r_W}{r_B} = 1 + \mathcal{O}\left[\left(\frac{\ell_{Pl}}{m}\right)^{\frac{2}{3}} \ln\left(\frac{m}{\ell_{Pl}}\right)\right]. \quad (5.25)$$

If we again consider a solar mass black hole, we have $r_W \approx (3 + \mathcal{O}(10^{-25}))$ km. Since we have a smooth effective geometry connecting the interior and asymptotic regions, which furthermore agrees with the Schwarzschild metric to an excellent degree of approximation, we can calculate the ADM mass of this solution. Since there is a time translation Killing field in the asymptotic region we can relate the radius of the black hole–type horizon to the ADM mass in asymptotic region I and the white hole–type horizon to the ADM mass of asymptotic region III of Fig. 4 (using Komar integrals discussed below.) Each of these two ADM masses is extremely well approximated by the radius of the corresponding horizon (divided by $2G$). Therefore, we conclude that for macroscopic black holes the ADM mass in all asymptotic regions are the same to an excellent approximation which, furthermore, improves as the mass increases.

(iii) Translational Killing vector and the Komar mass: By construction, the effective geometry admits a translational Killing field X^a which, as in the classical theory, is timelike in exterior regions and spacelike in the interior. Let us focus on the interior and calculate the Komar integrals

$$K_X[S] := -\frac{1}{8\pi G} \oint_S \epsilon_{ab}{}^{cd} \nabla_c X_d dS^{ab} \quad (5.26)$$

using various round 2-spheres S. Recall that, if S_1, S_2 are joined by a 3-surface M, then

$$K_X[S_2] - K_X[S_1] = 2 \int_M \left(\mathfrak{T}_{ab} - \frac{1}{2}\mathfrak{T} g_{ab}\right) X^a dV^b, \quad (5.27)$$

where dV^b is the oriented volume element of the 3-surface M. If we choose S to lie on a horizon, the Komar mass $K_X[S]$ is related to the horizon radius by $2GK_X[S] = r_{hor}$. Let S_1 lie on the black hole–type horizon and S_2 lie on the white hole–type horizon in the central diamond of Fig. 4 and M be a three-dimensional "tube" joining them. Then we appear to have a paradox. On the one hand, in the interior region there is an effective stress-energy tensor because the quantum corrected metric is not Ricci flat. Therefore, the integrand on the right side in (5.27) is nonzero. Indeed, the 3-surface M must cross the transition surface $\mathcal{T}$ and, as we saw in Sec. IV B, the energy density and pressures are quite large near the transition surface. Furthermore as Fig. 3 shows, both these quantities are negative almost everywhere in the interior (except near the horizon where their positive values are quite small). Therefore, one would expect the integral on the right side of (5.27) to be negative and rather large. How could the two horizons then have the same mass (to an excellent degree of approximation)?

The solution of this puzzle is conceptually interesting. The right-hand side of (5.27) is indeed negative and large. But the effective geometry is such that it is given by $-2M_B$, where $M_B = r_B/2G$. Therefore, while $K_X[S_1] = M_B$, we have $K_X[S_2] = -M_B$ (to an excellent degree of approximation). Geometrically, the negative sign arises simply because while the Killing vector X^a is future directed along the black hole–type horizon (and in the asymptotic region I), it is past directed along the white hole–type horizon (and in asymptotic region III). As is evident from Fig. 3, this must happen simply because the effective metric and its Killing field X^a are smooth. On the other hand, the ADM energy is defined at spatial infinity in each asymptotic region using the asymptotic Killing field which is *future directed and unit* at spatial infinity and is, thus, positive. Thus, the effective solution has the striking property it introduces just the right type of effective stress-energy that, on the one hand, large enough to resolve the singularity and, on the other, achieves the fine balance that is needed to satisfy the following relations:

$$M_{ADM}^{(I)} = M_{ADM}^{(III)} \quad \text{which requires} \quad K_X[S_2] = -K_X[S_1]. \quad (5.28)$$

Here $M_{ADM}^{(I)}$ is the ADM mass in the region I and $M_{ADM}^{(III)}$ the ADM mass in region III and $K_X[S_1]$ is the Komar integral on the black hole–type horizon and $K_X[S_2]$ on the

white hole–type horizon. It is thanks to this fine balance that there is no mass amplification in the large m limit.

VI. DISCUSSION

The issue of the fate of black hole singularities in quantum gravity has drawn a great deal of attention especially over the past two decades. While there is broad consensus that singularities are windows onto physics beyond Einstein's theory, there is no general agreement on how the singularities are to be resolved and even whether one should expect them to be resolved. For example, in the commonly used Penrose diagram of an evaporating black hole–first introduced by Hawking [42] over 40 years ago–a singularity constitutes part of the future boundary of spacetime even after the black hole has completely disappeared. Although this scenario is not based on a hard calculation in any approach to quantum gravity, it continues to be widely used. There is also a debate on whether quantum gravity effects associated with black holes would be important at horizons of macroscopic black holes and even in the exterior region well outside the horizons [39].

In this paper, we focused on a specific issue by restricting ourselves to the Kruskal spacetime: Is there a coherent, effective description that incorporates sufficient elements of a deeper quantum gravity theory to lead to the resolution of singularities of this spacetime? If there is, further questions arise. What is the nature of the resulting quantum extension? Do the large quantum gravity effects that are needed to resolve the central singularity persist even in low curvature regions, thereby modifying the classical geometry near and outside the black hole horizon? Is the quantum corrected effective geometry well defined both in the interior region bounded by horizons as well as the exterior asymptotic region? If the extension includes antitrapped regions, are they connected to new asymptotic regions? Is the ADM mass in these regions essentially the same as the initial mass one starts with or there is a significant mass inflation or deflation? We were able to answer these questions in detail within an effective theory that incorporates key elements of Riemannian quantum geometry underlying LQG.

The salient features of this effective description are the following. First, as shown in Secs. II and III, the black hole singularity is naturally resolved due to quantum geometry effects, i.e., because there is an area gap Δ in LQG. The singularity is replaced by a transition surface $\mathcal{T}$ which separates a trapped region to its past from the antitrapped region to its future: Our effective description extends the Schwarzschild interior to include a white hole–type horizon beyond the 'would be' singularity. Since the effective metric is smooth, all curvature invariants are bounded. Furthermore–as is common in loop quantum cosmology–each curvature invariant has an absolute upper bound that does not grow with mass (Sec. IV C). The expressions of

these upper bounds contain inverse powers of the area gap Δ. This is analogous to the observation—often emphasized by John Wheeler—that $\hbar$ appears in the denominator of the expression of the ground state energy of the hydrogen atom and the fact that it is nonzero prevents the minimum energy from being unbounded below. Thus, there is a precise and sharp sense in which singularity resolution is due to quantum geometry effects that give rise to a nonzero area gap. While quantum corrections lead to large violations of Einstein's equations near the transition surface (Sec. IV B) they become negligible in the low curvature region (Sec. IV D). In particular, for macroscopic black holes with $M \gg M_{\mathrm{Pl}}$, classical general relativity continues to provide an excellent approximation near and outside their horizons. While previous works focused only on the Schwarzschild interior, a key new feature of our analysis is that we were able to construct a Hamiltonian description and analyze effective dynamics also in the exterior region between the horizons and infinity (Sec. V A). These are joined in a smooth manner to the interior regions across horizons (Sec. V B), providing us with a quantum extension of the full Kruskal spacetime shown in Fig. 4.

There is a large body of work on the Kruskal interior within LQG [4–13], most of which focuses on effective dynamics as in this paper. In all these investigations, the black hole singularity is resolved. However, as discussed in Sec. IV D, there are also major differences from our approach. Physical results in [4,5,8] can depend on fiducial structures that are introduced in the construction of the classical phase space, whence the details of their predictions have no invariant significance. Our approach also starts with fiducial structures to make various mathematical expressions well defined. However, all our final results are insensitive to these choices. The final results in approaches introduced in [6,7,10,12] are also free of dependence on fiducial structures. However, they lead to large quantum effects in low curvature regions. For example, for large black holes, the quintessentially quantum transition surface $\mathcal{T}$ can emerge in regions with arbitrarily small curvature in some approaches [10], while quantum dynamics drives the effective trajectories to regions of phase space where the basic underlying assumptions are violated in others [6,7,13]. This does not occur in our approach. Indeed, this effective description is free from all known weaknesses of previous investigations of Kruskal spacetime within LQG.

Finally, another key difference from previous investigations is the following. They considered only the Schwarzschild interior and treated it as a homogeneous (Kantowski-Sachs) cosmology, emphasizing issues that are central to anisotropic cosmological models. For example some allowed matter [20,21] and/or a cosmological constant [9,11], thereby taking the focus away from the Schwarzschild interior. As mentioned already, our effective theory encompasses both the interior and the asymptotic regions and our focus is on black hole aspects such as

trapped and antitrapped surfaces in the interior region and properties of the ADM mass in the asymptotic region. A striking feature of this effective description is that, in the large mass limit, the ADM mass does not change as one evolves from one asymptotic region to another one to its future. This feature arises from a surprising aspect of the specific way Einstein's equations receive quantum corrections. On the one hand, these corrections are large enough to create a sufficiently strong repulsive behavior that is needed to resolve the singularity. On the other hand, in the evolution from the black hole–type horizon to the white hole–type horizon, the violation of Einstein's equations is subtle: the effective stress-energy induced by quantum geometry just flips the sign of Komar mass, keeping its magnitude the same. This flip goes hand in hand with the change of orientation of the translational Killing field, which in turn assures that the ADM mass remains the same from one asymptotic region to another one to its future (Sec. V B 2). This is why the geometry of the interior region is symmetric under time reflection around the transition surface $\mathcal{T}$ (in the large mass limit). A symmetric behavior has been sought after and achieved using phenomenological inputs before [12]; it has been postulated in studies on black hole to white hole transition [43]; and arrived at by imposing physically motivated conditions on the black hole evaporation time scale [44]. In our approach, it emerges from detailed effective dynamics and is more subtle. In particular, exact symmetry holds only in the infinite mass limit.

Our effective dynamics also provides a concrete context to compare and contrast expectations based on the quantum nature of Riemannian geometry a la LQG and those based on the AdS/CFT–type arguments. Since the bulk/boundary duality proposed in the AdS/CFT correspondence has been verified in a large number of examples, expected physical properties of quantum field theories on the boundary have been used to argue that quantum gravity will/should *not* resolve certain bulk singularities, including those of the classical Schwarzschild–anti–de Sitter spacetimes [26]. Note that these conclusions on the nature of bulk geometry are indirect in that they are arrived at starting from physically desirable properties of theories on the boundary, assuming the boundary/bulk correspondence. By contrast, in LQG, one works directly with the bulk. Since our effective theory does resolve Schwarzschild singularities in a coherent fashion, there is tension between the two sets of ideas. There is no contradiction since the plausibility arguments of [26] make a strong use of asymptotically anti–de Sitter boundary conditions and do not apply to the asymptotically flat situation we have considered. Therefore, it would be of interest to see if the effective theory proposed here can be extended to the asymptotically anti–de Sitter case. A result in either direction will provide valuable guidance.

We will conclude by pointing out some important limitations of our analysis. As in the previous investigations, it is straightforward to introduce the kinematical Hilbert space of states by exploiting the underlying homogeneity. Furthermore, using considerations of Appendix A, one can write down the quantum Hamiltonian constraint. However, its explicit action is rather complicated. The situation was initially the same with the 'improved dynamics' scheme in LQC, where it took some effort [28] to simplify the action of the Hamiltonian constraint sufficiently to make subsequent calculations manageable. The simplified form could then be used to arrive systematically at the quantum corrected, effective equations [3,18,19]. For the Kruskal black holes now under consideration, one would similarly have to first simplify the action of the Hamiltonian constraint significantly to 'derive' the effective equations proposed in this paper starting from the quantum theory. Secondly, the question of stability of our effective spacetimes has not been investigated. This is a difficult issue because we do not have quantum corrected equations for full general relativity. Nonetheless, since significant progress has been made on cosmological perturbations propagating on quantum FLRW geometries [1,45,46], it may be possible to analyze this issue in detail. A more important limitation comes from the fact that our analysis is confined to the *eternal* black-white holes of Kruskal spacetime. To address key conceptual issues such as the possibility of information loss, one would have to consider black holes formed by gravitational collapse. For these situations, as in classical general relativity, only a small part of the Penrose diagram of Fig. 4 will be relevant. One would have dynamical horizons which are either spacelike (in the classical phase when the black hole grows) or timelike (during the quantum evaporation process), rather than null as in the Kruskal picture considered here; only a finite portion of the transition surface will appear because of the black hole evaporation; and there will likely be only one asymptotic region (see, e.g., [47]). Thus, the conceptual structure of the framework would be very different from the full extension of Kruskal spacetime introduced here. Nonetheless, portion of this extended spacetime will be relevant to the analysis and may in fact suffice to address deep conceptual puzzles that arise already in the semi-classical regime, e.g., during the phase in which a solar mass black hole shrinks to lunar mass due to evaporation [48,49]. Furthermore, just as the analysis of quantum fields on Kruskal spacetime provided useful techniques in the analysis of the Hawking process for physically more realistic collapsing situations, techniques developed in this quantum extension of Kruskal spacetime should be helpful for the much more interesting physical problem of the fate of black hole singularities in dynamical processes.

APPENDIX A: QUANTUM PARAMETERS AS JUDICIOUSLY CHOSEN DIRAC OBSERVABLES

Given the quantum parameters δ_b, δ_c, the Hamiltonian constraint of the effective theory is given by [see (2.18)]

$$H_{\text{eff}} = -\frac{1}{2G\gamma}\left[\left(\frac{\sin(\delta_b b)}{\delta_b} + \frac{\gamma^2\delta_b}{\sin(\delta_b b)}\right)p_b + 2\frac{\sin(\delta_c c)}{\delta_c}p_c\right]$$

$$\equiv \frac{L_0}{G}[O_1 - O_2]. \tag{A1}$$

where $O_1 := -\frac{1}{2\gamma}\left[\frac{\sin\delta_b b}{\delta_b} + \frac{\gamma^2\delta_b}{\sin\delta_b b}\right]\frac{p_b}{L_o}$, and

$$O_2 := \left[\frac{\sin\delta_c c}{\gamma L_o\delta_c}\right]p_c. \tag{A2}$$

The task of making δ_b, δ_c constants of motion is technically subtle: δ_b, δ_c themselves feature in the expression (A1) of the Hamiltonian constraint that determines the dynamical trajectories along which δ_b, δ_c are to be constants. Thus, we have to choose δ_b, δ_c astutely to ensure this internal consistency. The goal of this Appendix is to show that these goals can be achieved and that the choice (4.6) made in Sec. IV A satisfies this subtle consistency.

To achieve this goal, we will proceed in the following steps: (1) We will first extend the four-dimensional phase space Γ of the main text (with canonically conjugate variables b, p_b, and c, p_c) to a eight-dimensional phase space Γ_{ext} by introducing 2 additional independent canonically conjugate pairs $\delta_b, p_{\delta b}$ and $\delta_c, p_{\delta c}$. Thus, in particular, on Γ_{ext}, the would-be quantum parameters δ_b and δ_c are not functions of $b, p_b; c, p_c$, but Poisson commute with all original phase space variables. (2) We will consider the natural lift $H_{\text{eff}}^{\text{ext}}$ of the Hamiltonian H_{eff} to Γ_{ext} and examine the Hamiltonian flow it generates. As we argue below, O_1, O_2 are Dirac observables for this flow. If δ_b is required to be a function only of O_1 and δ_c of only O_2 then δ_b, δ_c would also be Dirac observables. Our goal then is to introduce these dependences as two new constraints such that they, together with the Hamiltonian constraint function $H_{\text{eff}}^{\text{ext}}$ form a first class set on the extended phase space Γ_{ext}. Then, in

particular, the Hamiltonian flow generated by $H_{\text{eff}}^{\text{ext}}$ on the extended phase space Γ_{ext} will be tangential to the five-dimensional constraint surface $\bar{\Gamma}_{\text{ext}}$. (3) Finally, our goal is to choose two gauge fixing conditions for the newly introduced constraints such that the four-dimensional reduced phase $\hat{\Gamma}_{\text{ext}}$ corresponding to these constraints is symplectomorphic to the original four-dimensional phase space Γ we began with. The dynamical flow on $\bar{\Gamma}_{\text{ext}}$ would then be induced by the Hamiltonian $H_{\text{eff}}^{\text{ext}}$, but with δ_b, δ_c given by the specified functions of O_1 and O_2 respectively. Assuming all requirements on the choice of new constraints and their gauge fixing can be satisfied, the dynamical flow on $\bar{\Gamma}_{\text{ext}}$ will naturally descend to the constraint surface $\bar{\Gamma}$ of the original phase space Γ, providing us with the desired dynamics. Conditions in the second and third step are quite demanding and *a priori* it is not clear that they can be met. However, as we show below, there is a large class of choices of δ_b, δ_c for step (2) for they can be made. Among them is the choice (4.6) made in Sec. IV A. We will now carry out these three steps systematically.

The extended phase space Γ_{ext} is naturally coordinatized by four canonically conjugate pairs $b, p_b; c, p_c; \delta_b, p_{\delta b}; \delta_c, p_{\delta c}$. Note that δ_b, δ_c are just new, independent canonical variables that Poisson commute with the original $b, p_b; c, p_c$ and their conjugate momenta $p_{\delta_b}, p_{\delta_c}$ do not appear in the expression of

$$H_{\text{eff}}^{\text{ext}} = \frac{L_0}{G}[O_1 - O_2]. \tag{A3}$$

Since furthermore, O_1 refers only to the b-sector and O_2 only to the c-sector, it follows that O_1, O_2 Poisson commute and are, furthermore, Dirac observables of the flow generated by $H_{\text{eff}}^{\text{ext}}$ on Γ_{ext}. (As one would expect from our discussion in the main text, along dynamical trajectories O_2 equals O_1 and they will turn out to be the mass m. See Eq. (2.26).) To carry out steps (2) and (3) explicitly, it is convenient to first make a detour and introduce a canonical transformation so that O_1, O_2, δ_b, δ_c are the new configuration variables, and their momenta are given by:

$$P_1 = -\frac{2L_o}{Gb_o}\tanh^{-1}[b_o^{-1}\cos(\delta_b b)] - \frac{2L_o}{G}\ln\left|\frac{\gamma\delta_b}{2}\right|, \tag{A4}$$

$$P_2 = -\frac{L_o}{2G}\ln\left[\left|\frac{2p_c}{L_o\delta_c}\left[\frac{\sin\delta_c c}{\gamma L_o\delta_c}\right]\tan\left(\frac{\delta_c c}{2}\right)\right|\right], \tag{A5}$$

$$\begin{aligned}
P_{\delta_b} = p_{\delta_b} &- \frac{p_b}{2\gamma G}\left\{\frac{2}{\delta_b}\left[b - \left(\frac{\sin(\delta_b b)}{\delta_b} + \frac{\gamma^2\delta_b}{\sin(\delta_b b)}\right)\right]\right.\\
&+ \frac{\gamma}{b_o^2\sin(\delta_b b)}\left(2\gamma\cos(\delta_b b)\right.\\
&\left.\left. + \frac{\gamma}{b_o}\tanh^{-1}[b_o^{-1}\cos(\delta_b b)](2b_o^2 - 1 - \cos(2\delta_b b))\right)\right\},
\end{aligned} \tag{A6}$$

$$P_{\delta_c} = p_{\delta_c} - \frac{p_c}{2\gamma G \delta_c}\left(c - \frac{\sin(\delta_c c)}{\delta_c}\right). \qquad (A7)$$

Direct calculations show that Eqs. (A4)–(A7) define a canonical transformation on Γ_{ext} from the original variables $(b, p_b; c, p_c; \delta_b, p_{\delta_b}; \delta_c, p_{\delta_c})$ to $(O_1, P_1; O_2, P_2; \delta_b, P_{\delta_b}; \delta_c, P_{\delta_c})$:

$$\{O_i, P_j\} = \delta_{ij}, \quad \{\delta_b, P_{\delta_b}\} = 1, \quad \{\delta_c, P_{\delta_c}\} = 1, \qquad (A8)$$

and all remaining Poisson brackets vanish. This transformation is complicated in part because we have also ensured that it is well defined in the classical limit in which $\delta_b \to 0$ and $\delta_c \to 0$. This transformation is invertible and we provide the explicit inverse at the end of this Appendix.

The step (2) asks us to make δ_b, δ_c the desired functions of other phase space variables by introducing constraints on Γ_{ext}. Since in the final picture we would like δ_b, δ_c to be Dirac observables and since we know that O_1 and O_2 are Dirac observables, we choose these constraints to be:

$$\Phi_1 = O_1 - F_b(\delta_b) \approx 0, \quad \text{and} \quad \Phi_2 = O_2 - F_c(\delta_c) \approx 0, \qquad (A9)$$

where F_b and F_c are functions of δ_b, δ_c whose functional can be quite general, subject to suitable regularity conditions. (Our final choice (4.6) of these quantum parameters is of this form because, as noted above $O_1 = m = O_2$ on dynamical trajectories.) Since O_1, O_2 do not depend on the momenta $P_{\delta_b}, P_{\delta_c}$ of the quantum parameters δ_b, δ_c, it follows immediately that the three constraints $H_{\text{eff}}^{\text{ext}} \approx 0, \Phi_1 \approx 0, \Phi_2 \approx 0$ on Γ_{ext} constitute a first class system. Thus, we have met the conditions specified in step (2).

Next, consider the flow of the *total* Hamiltonian:

$$\begin{aligned} H_{\text{T}}^{\text{ext}} &= \underline{N} H_{\text{eff}}^{\text{ext}} + \lambda_1 \Phi_1 + \lambda_2 \Phi_2 \\ &= -\frac{L_o \underline{N}}{G}[O_2 - O_1] + \lambda_1[O_1 - F_b(\delta_b)] \\ &\quad + \lambda_2[O_2 - F_c(\delta_c)], \end{aligned} \qquad (A10)$$

where $\underline{N}, \lambda_1, \lambda_2$ are Lagrange multipliers. The equations of motion defined by the Hamiltonian flow of H_T^{ext} are

$$\dot{O}_1 = 0, \quad \dot{P}_1 = -\frac{L_o \underline{N}}{G} - \lambda_1; \quad \dot{O}_2 = 0, \quad \dot{P}_2 = \frac{L_o \underline{N}}{G} - \lambda_2; \qquad (A11)$$

$$\dot{\delta}_b = 0, \quad \dot{P}_{\delta_b} = \lambda_1 F_b'(\delta_b); \quad \dot{\delta}_c = 0, \quad \dot{P}_{\delta_c} = \lambda_2 F_c'(\delta_c); \qquad (A12)$$

and, in addition, the phase space variables are subject to the three constraints:

$$O_1 - O_2 = 0, \quad O_1 - F_b(\delta_b) = 0, \quad O_2 - F_c(\delta_c) = 0. \qquad (A13)$$

The equations are, thus, very simple; this is the reason why we introduced the new canonical variables. We know from general arguments that the flow is tangential to the five-dimensional constraint surface $\bar{\Gamma}_{\text{ext}}$ in Γ_{ext}. Equations of motion make this explicit.

Remark: The explicit form of solutions implies that δ_b, δ_c are constants along dynamical trajectories, as desired. Furthermore, for any choice of (regular) functions F_b, F_c, their explicit dependence on the new configuration variables O_1 is known. The construction of Sec. IV A led us to set

$$F_b(\delta_b) = \left(\frac{\sqrt{\Delta}}{\sqrt{2\pi}\gamma^2 \delta_b^3}\right), \qquad F_c(\delta_c) = \frac{1}{8}\left(\frac{\gamma \Delta^2}{4\pi^2 (L_o \delta_c)^3}\right), \qquad (A14)$$

but the main conclusions of this Appendix do not require this specific choice. Discussion of the causal structure of the Kruskal interior of Sec. III holds for the class of quantum parameters that correspond to general F_b and F_c– and these include the choices made in the generalized μ_o approaches [10,12] discussed in Sec. IV D 3.

But we still need to relate the dynamical trajectories on $\bar{\Gamma}_{\text{ext}}$ to those on the constraint surface $\bar{\Gamma}$ of the original phase space Γ. This requires completion of step (3) of the program: Introduction of gauge fixing for the new constraints $\Phi_1 \approx 0$ and $\Phi_2 \approx 0$ so that the resulting four-dimensional reduced phase space $\hat{\Gamma}_{\text{ext}}$ is symplectomorphic to the original phase space Γ spanned by $b, p_b c, p_c$. This means that the gauge fixing conditions should be such that the terms

$$(d\delta_b \wedge dP_{\delta_b} + d\delta_c \wedge dP_{\delta_c}) \qquad (A15)$$

in the expression of the symplectic structure on Γ_{ext} should vanish when pulled back to $\hat{\Gamma}_{\text{ext}}$. An examination of the form of the constraints leads us to conditions of the form

$$P_{\delta_b} = G_b(O_1, O_2), \qquad P_{\delta_c} = G_c(O_1, O_2),$$

$$\text{such that} \quad \frac{1}{F_b'(\delta_b)}\frac{\partial G_b}{\partial O_2} = \frac{1}{F_c'(\delta_c)}\frac{\partial G_c}{\partial O_1}. \qquad (A16)$$

The form of the evolution equations implies that these are good gauge fixing conditions in the sense that each gauge orbit generated by the new constraint functions Φ_1 and Φ_2 intersects the gauge fixed surface once and only once. Finally evolution consistent with this gauge fixing is obtained by setting $\lambda_1 = \lambda_2 = 0$ in the expression (A10) of H_T^{ext}. Thus, we have exhibited a family of gauge conditions satisfying conditions (3) in our prescription.

On the four-dimensional reduced phase space $\hat{\Gamma}_{\text{ext}}$, then, dynamics is generated by the Hamiltonian constraint $H_{\text{eff}}^{\text{ext}}$ of (A3) where, now, δ_b, δ_c are determined by the constraints $\Phi_1 = 0$ and $\Phi_2 = 0$. The explicit form of this evolution is given by the restriction of (A11) and (A12) to the constraint surface $H_{\text{eff}}^{\text{ext}} = 0$ of the reduced phase space $\hat{\Gamma}_{\text{ext}}$. Evolution of P_1, P_2 is extremely simple, and O_1, $O_2; \delta_b, \delta_c$ are constants of motion related via constraints $\Phi_1 = 0, \Phi_2 = 0$.

Finally, one can rewrite these evolution equations in terms of $b, p_b; c, p_c$ by using the inverse of the canonical transformations (A4)–(A7) on Γ_{ext}:

$$\cos(\delta_b b) = -b_o \tanh\left[\frac{b_o}{2}\left(\frac{GP_1}{L_o} + 2\ln\left|\frac{\gamma\delta_b}{2}\right|\right)\right], \qquad \text{(A17)}$$

$$\frac{b_o^2}{2L_o\gamma}p_b = -\delta_b O_1 b_o^2 \cosh\left[\frac{b_o}{2}\left(\frac{GP_1}{L_o} + 2\ln\left|\frac{\gamma\delta_b}{2}\right|\right)\right]^2$$
$$\times \sqrt{1 - b_o^2 \tanh\left[\frac{b_o}{2}\left(\frac{GP_1}{L_o} + 2\ln\left|\frac{\gamma\delta_b}{2}\right|\right)\right]^2}, \qquad \text{(A18)}$$

$$\tan\left(\frac{\delta_c c}{2}\right) = \pm\frac{L_o\delta_c}{2O_2}e^{-2GP_2/L_o}, \qquad \text{(A19)}$$

$$p_c = \gamma O_2^2\left(e^{2GP_2/L_o} + \frac{L_o^2\delta_c^2}{4O_2^2}e^{-2GP_2/L_o}\right). \qquad \text{(A20)}$$

(In the effective theory, the phase space Γ_{ext} is restricted such that $c \in [-\pi/\delta_c, 0) \cup (0, \pi/\delta_c]$ and $b \in [-\pi/\delta_b, 0) \cup (0, \pi/\delta_b]$ [see footnote 6].) The resulting equations of motion for $b, p_b; c, p_c$ are precisely Eqs. (2.19) and (2.20) of the main text.

Remark: The Hamiltonian constraint (A1) can be formally promoted to an operator $\hat{H}$ on the Kinematical Hilbert space $\mathcal{H}_{\text{kin}}$ used in the literature (see, e.g., [4,10]), but its explicit action on the basis states normally used is rather complicated because δ_b, δ_c depend on the phase space variables via Eq. (4.6). A possible avenue to simplify the action is suggested by the strategy adopted in this Appendix. One may extend the kinematical Hilbert space by introducing new degrees of freedom corresponding to δ_b, δ_c (and their canonically conjugate variables) also in the quantum theory, and then impose the three first class constraints as operator equations on the extended kinematical Hilbert space $\mathcal{H}_{\text{kin}}^{\text{ext}}$. This step would be straightforward, e.g., if one uses the representation in which p_b, p_c, δ_b, δ_c are diagonal. However, further work is need to first explicitly solve the new operator constraints $\hat{\Phi}_i = 0$ since δ_b, δ_c also appear in the expressions of $\hat{O}_i$ ($i = 1, 2$). One possibility is to first seek the generator of the canonical transformations (A4)–(A5), promote it to an operator to go back and forth between representations in which p_b, p_c, δ_b, δ_c are diagonal and the one in which O_1, O_2, δ_b, δ_c

(or, P_1, P_2, δ_b, δ_c) are diagonal and exploit the simplicity of constraints in terms of O_1, O_2, δ_b, δ_c.

APPENDIX B: DETERMINING THE QUANTUM PARAMETERS δ_b AND δ_c

Results of Appendix A hold for a judiciously chosen but still a large class of the quantum parameters δ_b, δ_c. In the main body of the paper, we used a specific form (4.6). In this Appendix, we derive this equation starting from conditions (4.4) and (4.5) on the area enclosed by the chosen plaquettes on the transition surface $\mathcal{T}$. We will first derive analytical expressions in the large m limit and then discuss some subtleties associated with the exact solutions. The strategy is to first obtain expressions of $p_b|_{\mathcal{T}}$ and $p_c|_{\mathcal{T}}$ at the transition surface $\mathcal{T}$ as functions of δ_b, δ_c using explicit solutions (2.25) and (2.22) to effective equations, and then determine the two unknowns δ_b, δ_c using the two area conditions (4.4) and (4.5).

The expression of p_c at the transition surface is simple: $p_c|_{\mathcal{T}} = m(\gamma L_o\delta_c)$. By contrast, the expression of $p_b|_{\mathcal{T}}$ is intricate and far more nontrivial. To gain control over this expression, let us first consider an expansion in the limit $\delta_b \ll 1$ and $L_o\delta_c \ll \sqrt{\Delta}$. The leading order gives $p_b|_{\mathcal{T}} \simeq L_o(2m^3 L_o\gamma\delta_c)^{1/4}$. Then, we can solve Eqs. (4.4) and (4.5), and obtain

$$\delta_b \propto \left(\frac{\sqrt{\Delta}}{m}\right)^{1/3} \quad \text{and} \quad \frac{L_o\delta_c}{\sqrt{\Delta}} \propto \left(\frac{\sqrt{\Delta}}{m}\right)^{1/3}. \quad \text{(B1)}$$

(Recall that it is the combination $L_o\delta_c$ that is invariant under the rescaling $L_o \to \alpha L_o$ of the fiducial cell.) These conditions imply that δ_b and $L_o\delta_c$ are Dirac observables: they are constant on a given solution, but they can change from one solution to another. Our initial assumption $\delta_b \ll 1$ and $L_o\delta_c \ll \sqrt{\Delta}$ is automatically satisfied in the desired large m limit, $m \gg m_{\text{Pl}}$, if we set

$$\delta_b = A\left(\frac{\sqrt{\Delta}}{m}\right)^{1/3} \quad \text{and} \quad \frac{L_o\delta_c}{\sqrt{\Delta}} = B\left(\frac{\sqrt{\Delta}}{m}\right)^{1/3}, \quad \text{(B2)}$$

where A and B are some dimensionless constants (independent of the mass m) which get determined from the minimum area conditions.

Using Eq. (4.5) we find that A and B are related via

$$B = \frac{1}{4\pi\gamma A^2}, \quad \text{(B3)}$$

enabling us to trade B for A. Finally, to determine A we use the expression of $p_b|_{\mathcal{T}}$ and (B3). A straightforward computation provides us with an equation for A in the large m limit:

$$\frac{A^{3/2}\gamma}{2^{1/4}(4\pi)^{3/4}} + \frac{2^{1/4}}{(4\pi)^{5/4}A^{3/2}\gamma} = \frac{1}{2\pi}. \quad \text{(B4)}$$

This equation has only one real solution given by

$$A = \left(\frac{1}{\sqrt{2\pi}\gamma^2} \right)^{1/3} \tag{B5}$$

which then determines B via (B3)

$$B = \frac{1}{2} \left(\frac{\gamma}{4\pi^2} \right)^{1/3}. \tag{B6}$$

One can easily see that these values of A and B, together with (B2) provide the expression (4.6) of δ_b, δ_c

$$\delta_b = \left(\frac{\sqrt{\Delta}}{\sqrt{2\pi}\gamma^2 m} \right)^{1/3}, \qquad L_o\delta_c = \frac{1}{2} \left(\frac{\gamma\Delta^2}{4\pi^2 m} \right)^{1/3}. \tag{B7}$$

given in the main text. Thus, in the $m \gg \ell_{\rm Pl}$ limit, solutions to the area conditions (4.4) and (4.5) are given by (4.6) to leading order. Finally, it is instructive to solve Eq. (4.5) numerically, without taking the large m limit. Since we know $p_c|_{\mathcal{T}} = m(\gamma L_o\delta_c)$, let us start by first solving Eq. (4.5) for $L_o\delta_c$ and use the solution in Eq. (4.4). Then the only unknown in the solution (2.25) for p_b is δ_b. Therefore, we can numerically evaluate the left side $p_b(T_{\mathcal{T}})\delta_b\delta_c$ of (4.4) as a function of δ_b. The solid curve in Fig. 5 plots this function for $m = 10^4$. The right side of (4.4) is a constant, $\Delta/2\pi$, shown by the dashed line. The two curves have four intersections that represent four roots of our equation for δ_b. (Thus, if we do not take the large m limit, the two conditions (4.4) and (4.5) do not quite determine the unknowns δ_b, δ_c uniquely; we are left with a discrete, 4-parameter family of degeneracy.) We will refer to the four roots as the leftmost, the two central and the rightmost. Their properties can be summarized as follows. The two central roots are the relevant ones for our analysis. In the large mass limit, they approach each other and rapidly converge to a single degenerate value, given by the analytic expression (4.6). This root corresponds to the large m values of constants A and B given in (B5) and (B6). For macroscopic black holes
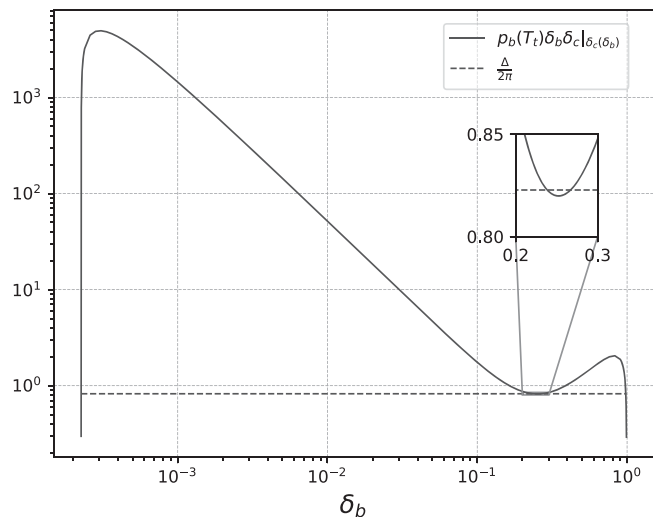

FIG. 5. The roots of δ_b obtained from solving Eqs. (4.4) and (4.5). In the large m limit, the central roots are extremely well approximated by Eqs. (B5) and (B6). The leftmost and rightmost roots turn out to have unphysical properties.

it is these central roots that yield the effective geometries discussed in Secs. IV B and IV C.

The leftmost and the rightmost roots, on the other hand, are unphysical. The leftmost root gives a value for δ_b that decreases rapidly as a function of the mass (faster than $m^{-1/3}$) while δ_c grows monotonically. In this case, the effective dynamics results in large quantum corrections at the black hole–type horizon. For the rightmost root, both δ_b and δ_c decrease with the mass, however δ_b does it very slowly. Although quantum corrections are small close to the black hole–type horizon, they grow very quickly and become important while the Kretschmann scalar is still small. Thus, the leftmost and the rightmost roots can not yield physically viable solutions. That is why we focused on the limiting value of the central roots in our analysis in the main text. Finally, for macroscopic black holes, the two central roots are extremely close to one another, whence corrections to the asymptotic value are negligible.

[1] *Loop Quantum Gravity: The First 30 Years*, edited by A. Ashtekar and J. Pullin (World Scientific, Singapore, 2017).

[2] P. Singh, Are loop quantum cosmologies never singular?, Classical Quantum Gravity **26**, 125005 (2009).

[3] A. Ashtekar and P. Singh, Loop quantum cosmology: A status report, Classical Quantum Gravity **28**, 213001 (2011).

[4] A. Ashtekar and M. Bojowald, Quantum geometry and the Schwarzschild singularity, Classical Quantum Gravity **23**, 391 (2006).

[5] L. Modesto, Loop quantum black hole, Classical Quantum Gravity **23**, 5587 (2006).

[6] C. G. Boehmer and K. Vandersloot, Loop quantum dynamics of Schwarzschild interior, Phys. Rev. D **76**, 1004030 (2007).

[7] D. W. Chiou, Phenomenological loop quantum geometry of the Schwarzschild black hole, Phys. Rev. D **78**, 064040 (2008).

[8] M. Campiglia, R. Gambini, and J. Pullin, Loop quantization of a spherically symmetric mid-superspaces: The interior problem, AIP Conf. Proc. **977**, 52 (2008).

[9] J. Brannlund, S. Kloster, and A. DeBenedictis, The evolution of Λ black holes in the mini-superspace approximation of loop quantum gravity, Phys. Rev. D **79**, 084023 (2009).

[10] A. Corichi and P. Singh, Loop quantum dynamics of Schwarzschild interior revisited, Classical Quantum Gravity **33**, 055006 (2016).

[11] N. Dadhich, A. Joe, and P. Singh, Emergence of the product of constant curvature spaces in loop quantum cosmology, Classical Quantum Gravity **32**, 185006 (2015).

[12] J. Olmedo, S. Saini, and P. Singh, From black holes to white holes: A quantum gravitational symmetric bounce, Classical Quantum Gravity **34**, 225011 (2017).

[13] J. Cortez, W. Cuervo, H. A. Morales-Tcotl, and J. C. Ruelas, On effective loop quantum geometry of Schwarzschild interior, Phys. Rev. D **95**, 064041 (2017).

[14] D. Cartin and G. Khanna, Wave functions for the Schwarzschild black hole interior, Phys. Rev. D **73**, 104009 (2006).

[15] M. Bojowald, D. Cartin, and G. Khanna, Lattice refining loop quantum cosmology, anisotropic models and stability, Phys. Rev. D **76**, 064018 (2007).

[16] S. Sabharwal and G. Khanna, Numerical solutions to lattice-refined models in loop quantum cosmology, Classical Quantum Gravity **25**, 085009 (2008).

[17] A. Yonika, G. Khanna, and P. Singh, Von-Neumann stability and singularity resolution in loop quantized Schwarzschild black hole, Classical Quantum Gravity **35**, 045007 (2018).

[18] J. Willis, On the low energy ramifications and a mathematical extension of loop quantum gravity, Ph.D. dissertation, The Pennsylvaina State University, 2004.

[19] V. Taveras, LQC corrections to the Friedmann equations for a universe with a free scalar field, Phys. Rev. D **78**, 064072 (2008).

[20] D-W. Chiou, Phenomenological dynamics of loop quantum cosmology in Kantowski-Sachs spacetime, Phys. Rev. D **78**, 044019 (2008).

[21] A. Joe and P. Singh, Kantowski-Sachs spacetime in loop quantum cosmology: Bounds on expansion and shear scalars and viability of quantization prescriptions, Classical Quantum Gravity **32**, 015009 (2015).

[22] S. Saini and P. Singh, Geodesic completeness and the lack of strong singularities in effective loop quantum Kantowski-Sachs spacetime, Classical Quantum Gravity **33**, 245019 (2016).

[23] R. Gambini, J. Omedo, and J. Pullin, Quantum black holes in loop quantum gravity, Classical Quantum Gravity **31**, 095009 (2014).

[24] R. Gambini and J. Pullin, Hawking radiation from a spherical loop quantum gravity black hole, Classical Quantum Gravity **31**, 115003 (2014).

[25] M. Campiglia, R. Gambini, J. Olmedo, and J. Pullin, Quantum self-gravitating collapsing matter in a quantum geometry, Classical Quantum Gravity **33**, 18LT01 (2016).

[26] N. Englehardt and G. T. Horowitz, New insights into quantum gravity from gauge/gravity duality, Int. J. Mod. Phys. D **25**, 1643002 (2016).

[27] T. Schilling, Geometry of quantum mechanics, Ph.D. dissertation, The Pennsylvania State University, 1996;

A. Ashtekar and T. A. Schilling, Geometrical formulation of quantum mechanics, in *On Einstein's Path: Essays in Honor of Engelbert Schücking*, edited by A. Harvey (Springer, New York, 1999), pp. 23–65.

[28] A. Ashtekar, T. Pawlowski, and P. Singh, Quantum nature of the big bang: Improved dynamics, Phys. Rev. D **74**, 084003 (2006).

[29] P. Diener, B. Gupt, and P. Singh, Numerical simulations of a loop quantum cosmos: Robustness of the quantum bounce and the validity of effective dynamics, Classical Quantum Gravity **31**, 105015 (2014).

[30] P. Diener, B. Gupt, M. Megevand, and P. Singh, Numerical evolution of squeezed and non-Gaussian states in loop quantum cosmology, Classical Quantum Gravity **31**, 165006 (2014).

[31] P. Diener, A. Joe, M. Megevand, and P. Singh, Numerical simulations of loop quantum Bianchi-I spacetimes, Classical Quantum Gravity **34**, 094004 (2017).

[32] J. Lewandowski, A. Okolow, H. Sahlmann, and T. Thiemann, Uniqueness of diffeomorphism invariant states on holonomy flux algebras, Commun. Math. Phys. **267**, 703 (2006).

[33] C. Fleishchack, Representations of the Weyl algebra in quantum geometry, Commun. Math. Phys. **285**, 67 (2009).

[34] A. Ashtekar and M. Campiglia, On the uniqueness of kinematics of loop quantum cosmology, Classical Quantum Gravity **29**, 242001 (2012).

[35] J. Engle, M. Hanusch, and T. Thiemann, Uniqueness of the representation in homogeneous isotropic LQC, Commun. Math. Phys. **354**, 231 (2017).

[36] A. Ashtekar and J. Lewandowski, Background independent quantum gravity: A status report, Classical Quantum Gravity **21**, R53 (2004).

[37] A. Ashtekar, M. Bojowald, and J. Lewandowski, Mathematical structure of loop quantum cosmology., Adv. Theor. Math. Phys. **7**, 233 (2003).

[38] A. Ashtekar, Loop quantum cosmology: An overview, Gen. Relativ. Gravit. **41**, 707 (2009).

[39] S. B. Giddings, Observational strong gravity and quantum black hole structure, Int. J. Mod. Phys. D **25**, 1644014 (2016).

[40] A. Ashtekar, T. Pawlowski, and P. Singh, Quantum nature of the big bang: An analytical and numerical investigation, Phys. Rev. D **73**, 124038 (2006).

[41] H. Liu and K. Noui, Gravity as an $su(1, 1)$ gauge theory in four dimensions, Classical Quantum Gravity **34**, 135008 (2017).

[42] S. W. Hawking, Particle creation by black holes, Commun. Math. Phys. **43**, 199 (1975).

[43] H. M. Haggard and C. Rovelli, Black hole fireworks: Quantum-gravity effects outside the horizon spark black to white hole tunneling, Phys. Rev. D **92**, 104020 (2015).

[44] E. Bianchi, M. Christodoulou, F. D'Ambrosio, H. M. Haggard, and C. Rovelli, White holes as remnants: A surprising scenario for the end of a black hole, Classical Quantum Gravity **35**, 225003 (2018).

[45] A. Ashtekar, Symmetry reduced loop quantum gravity: A bird's eye view, Int. J. Mod. Phys. D **25**, 1642010 (2016).

[46] I. Agullo and P. Singh, Loop quantum cosmology: A brief review, in *Loop Quantum Gravity: The first 30 Years*, edited by A. Ashtekar and J. Pullin (World Scientific, Singapore, 2017).

[47] A. Ashtekar and M. Bojowald, Black hole evaporation: A paradigm, Classical Quantum Gravity **22**, 3349 (2005).

[48] A. Ashtekar, The issue of information loss: The current status, ILQG Seminar of February 23rd, 2015 (2015), http://relativity.phys.lsu.edu/ilqgs/ashtekar022316.pdf.

[49] M. Christodoulou and T. De Lorenzo, On the volume inside old black holes, Phys. Rev. D **94**, 104002 (2016).